1-1-1978

Study of a centrifugal fluidized bed with solids feed and removal.

Seyed Mohammad Hashemi

STUDY OF A CENTRIFUGAL FLUIDIZED BED WITH SOLIDS FEED AND REMOVAL

Seyed Mohammad Reza Hashemi

Department of Mechanical Engineering
and Mechanics
Lehigh University
Bethlehem, Pennsylvania 18015

March 1978

This thesis is accepted and approved in partial fulfillment of the requirements for the degree of Master of Science.

3/22/78
(date)

Professor Edward K. Levy
Professor in Charge

Professor Douglas E. Abbott
Chairman of Department

TABLE OF CONTENTS

LIST OF TABLES

LIST OF FIGURES

LIST OF APPENDICES

NOMENCLATURE

SYMBOL	DESCRIPTION
dp	Particle diameter
$\overline{dp}$	Mean particle diameter
Ga	Modified Galileo number = $\frac{\rho_s(\rho_s - P_f)\omega^2 r_o dp^3}{\mu^2}$
g	Local acceleration of gravity (9.805 m/s^2)
H	Distance from chamber floor to ceiling
h	Distance above floor of chamber
h'	Maximum bed height above chamber floor
L	Depth of the bed
M	Mass of solids
M_B	Bed mass
M_C	Mass of collected particles
$\dot{M_A}$	Air flow rate m^3/s
$\dot{M_H}$	Mass flow rate of fluid per unit height of distributor
$\dot{M_S}$	Solids feed rate (Kg/s)
P	Pressure
r	Radius from axis of rotation
r_c	Radius to viscous core boundary
Re_{MF}	Minimum fluidization Reynolds number = $\frac{\rho_f U_{MF} \overline{dp}}{\mu}$
Rep	Particle Reynolds number = $\frac{\rho_f U_o dp}{\mu}$
r_f	Radius from axis of rotation to bed surface
r_o	Radius from axis of rotation to the grid surface

r_{o1}	Radius to grid surface at chamber floor
r_{o2}	Radius to grid surface at chamber ceiling
U_{MF}	Minimum fluidization velocity
U_o	Superficial gas velocity at $r=r_o$
V_θ	Tangential velocity
Z	Height above chamber floor
α	Grid wall inclination to vertical (taper angle)
ΔP_B	Bed pressure drop
ΔP_{BF}	Fluidized bed pressure drop
ΔP_{BMF}	Fluidized bed pressure drop at minimum fluidization
ΔP_{BP}	Packed bed pressure drop
ΔP_{ℓ}	Flow center line kinetic pressure
ΔP_G	Grid pressure drop
ΔP_{GFM}	Grid pressure drop at minimum fluidization air flow rate
ΔP_o	Overall pressure drop
ϵ	Void fraction
ϕ_s	Sphericity of particle
μ	Fluid viscosity
ω	Angular velcoity
ρ_f	Fluid density
ρ_s	Particle density
θ	Angle between verticle and the artificial horizon.

ABSTRACT

The effects of solids feeding and removal on the bed mechanics in a centrifugal fluidized bed (CFB) are investigated. The emphasis with this system is on the use of centrifugal fluidized beds (CFB) for combustion applications where with bed material of dolomite or limestone to capture SO_2, the centrifugal combustor could be used to burn high sulfur coal or coal char.

A centrifugal fluidized bed is cylindrical in shape and rotates about its axis of symmetry. As a consequence of the circular motion, the bed material is forced into the annular region at the circumference of the container, and fluid flows radially inward through the porous surface of the cylindrical distributor, fluidizing the bed material against the centrifugal forces generated by the rotation.

Room temperature experiments were performed with glass bed material, and the data from a series of batch experiments on bed pressure drop and minimum fluidization are compared with the theoretical expressions. Experiments also were performed to study bed operation with continuous feed and removal of bed material, and data on the effects of air flow rate, angular velocity, parti-

cle feed rate, and discharge geometry on bed pressure drop are presented.

I. INTRODUCTION

With increasing consumption of energy and decreasing resources of oil and natural gas, the world is faced with an energy problem which is often termed the "Energy Crisis". It is a generally accepted conclusion that energy demands by the end of this century will be enormous by present standards. Figure 1 shows the distribution of U.S. energy consumption in 1970 and the dependence of the U.S. on oil and natural gas. New solutions to energy use that are sound technically, socially and economically are becoming more and more important.

There are several alternatives to supply the energy man-needs, one of which is coal. However, the use of coal raises a problem of SO_2 pollution. The questions of how to satisfy the forthcoming SO_2 emission standards is an important part of the problem of fuels and energy management. Coal and oil combustion now contribute about 77 percent of the manmade SO_2 emission in the United States (65 percent from coal, 12 percent from oil) with about 55 percent of the total coming from power plants[1]. In view of the rapidly growing demand for electric power, two-thirds of the total SO_2 emissions in 1980 (estimated in 1971) are expected to originate from this source[1].

Figure 2 shows the use of oil is projected to in-

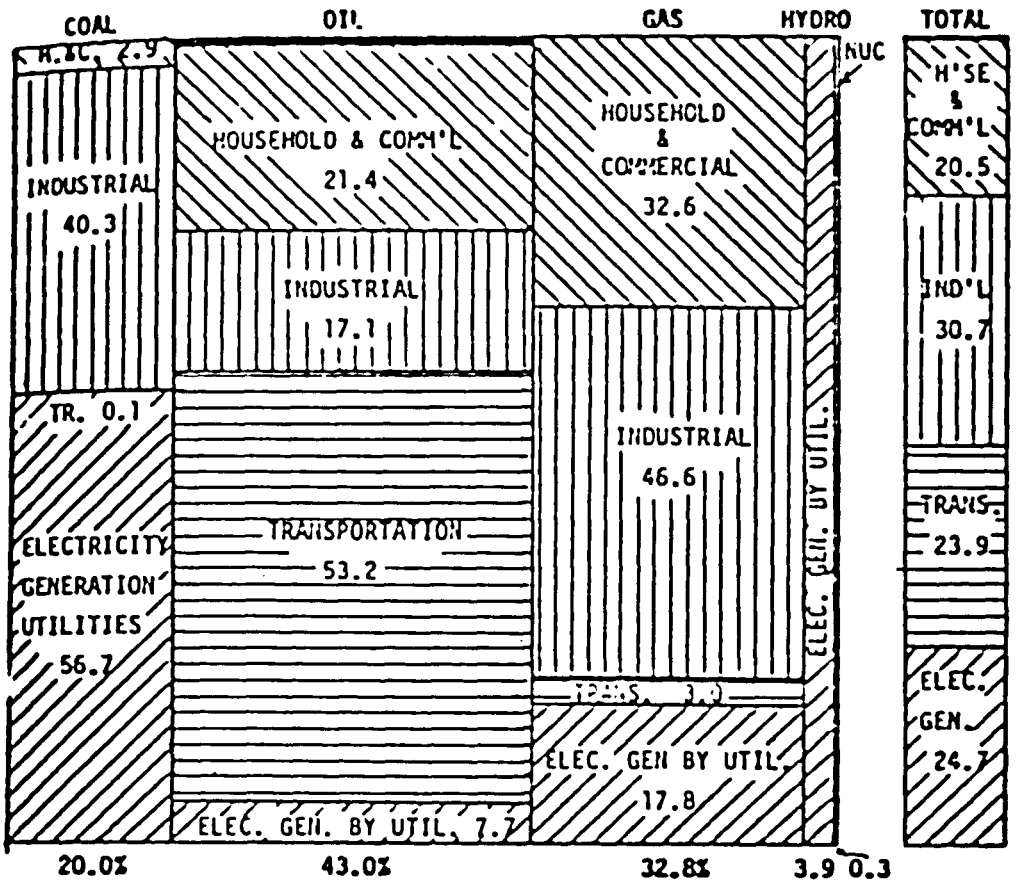

Fig. 1 Distribution of U.S. Energy Consumption, 1970 (Preliminary Estimates by U.S. Department of the Interior) [From Ref. 1]

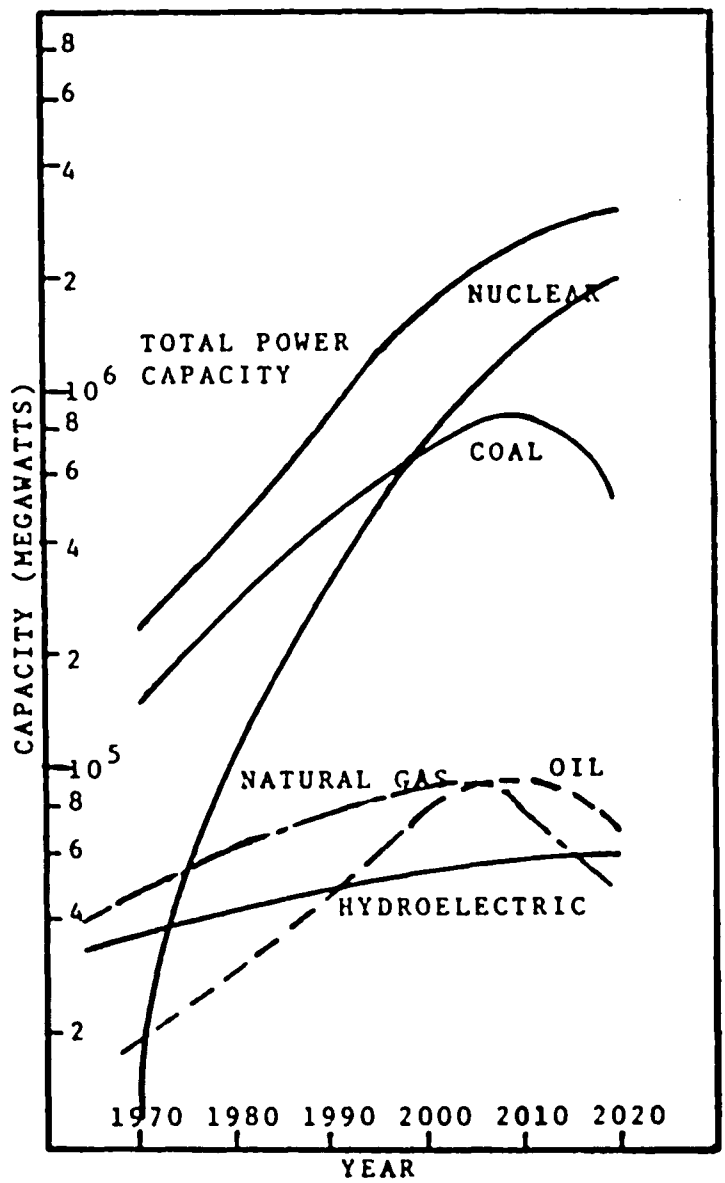

Fig. 2 Projected Power Generating Capacity and Fuel Sources of Electric Utilities in the U.S. (with Breeder) (NAE-NRC, 1970)

crease until its forecasted availability falls off around the year 2000. Natural gas usage also is expected to increase and then fall off sooner than oil. Hydroelectric sources are expected to remain relatively small. Nuclear generating capacity is increasing rapidly, but its impact will probably not prevent the power industry from being primarily dependent upon coal until the end of the century. Consequently, projections can be made for sulfur dioxide emissions from power plants if no abatement procedures are used. Table 1 shows the estimated potential sulfur dioxide pollution in the United States without abatement. The emission rate of SO_2 in 1990, if uncontrolled, might be over three times the rate in 1971[1].

One way to control SO_2 emissions from combustion of coal is through sulfur removal during combustion. To do this, the coal is burned in the presence of a sulfur acceptor. One process burns the coal in a fluidized bed of limestone particles which reacts with the sulfur. In this system a portion of the bed is continuously removed and replaced with fresh limestone.

A. Fluidized Bed Combustion

Research on fluidized bed combustion was started to obtain high heat transfer rates in boilers. The work on

Table 1 Estimated Potential Sulfur Dioxide Pollution in the United States without Abatement[a] (NAE-NRC, 1970)

Source	Annual Emission of Sulfur Dioxide (millions of tons) 1967	1970	1980	1990	2000
Power Plant Operation (Coal and Oil)	15.0	20.0	41.1	62.0	94.5
Other Combustion of Coal	5.1	4.8	4.0	3.1	1.6
Combustion of Petroleum Products (Excluding Power Plant Oil)	2.8	3.4	3.9	4.3	5.1
Smelting of Metallic Ores	3.8	4.0	5.3	7.1	9.6
Petroleum Refinery Operation	2.1	2.4	4.0	6.5	10.5
Miscellaneous Sources[b]	2.0	2.0	2.6	3.4	4.5
Total	30.8	36.6	60.9	86.4	125.8

a February 1970 NAPCA estimates, excluding transportation

b Includes coke processing, sulfuric acid plants, coal refuse banks, refuse incineration, and pulp and paper manufacturing.

modular construction by Pope Evans and Robins[2] has taken on the added burden of removing sulfur by fluidizing limestone along with the coal. There are many other organizations which have started working on developing fluidized bed combustion systems.

A fluidized bed is a two phase system composed of bulk solids and fluid in relative motion. When the velocity of the fluid through the bed bulk solids is such that the pressure drop of the fluid through the bed, due to viscous are inertia effects, is in equilibrium with the opposing pressure drop caused by the weight of the solids minus their buoyancy in the fluid, the bed is said to be in a fluidized condition.

In a conventional stationary fluidized bed (Figure 3) which Pope Evans and Robins started their work on, the weight of the solids is a function only of the bed mass, since the local acceleration of gravity is constant. In this case, the minimum fluidization velocity is defined as the velocity of the fluid when the pressure drop due to viscous and inertia effects can support the weight of the bed.

There is ample experience in the process industries to appreciate that fluidized bed combustors have lower volumes and higher heat transfer coefficients than con-

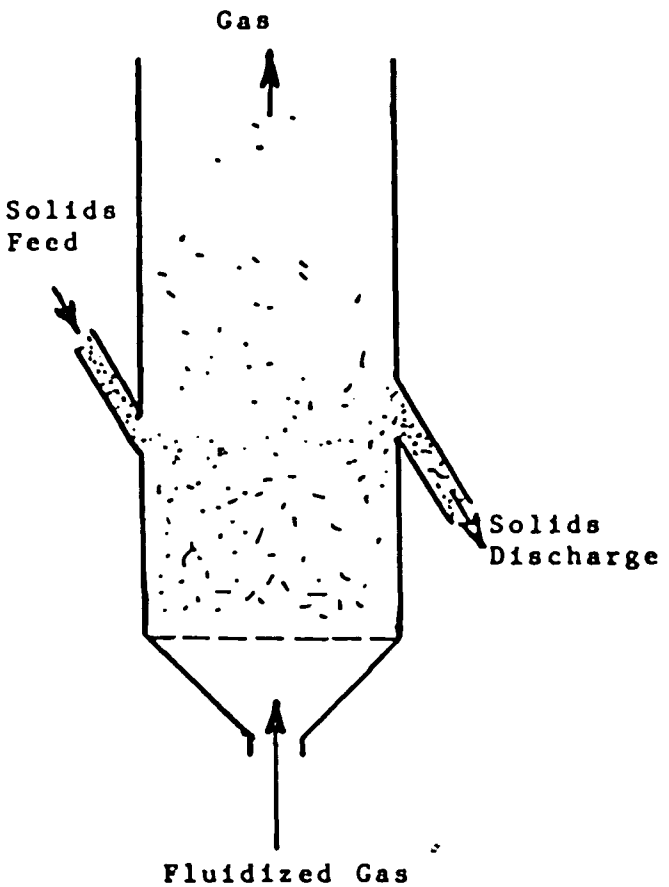

Fig. 3 A Conventional Fluidized Bed

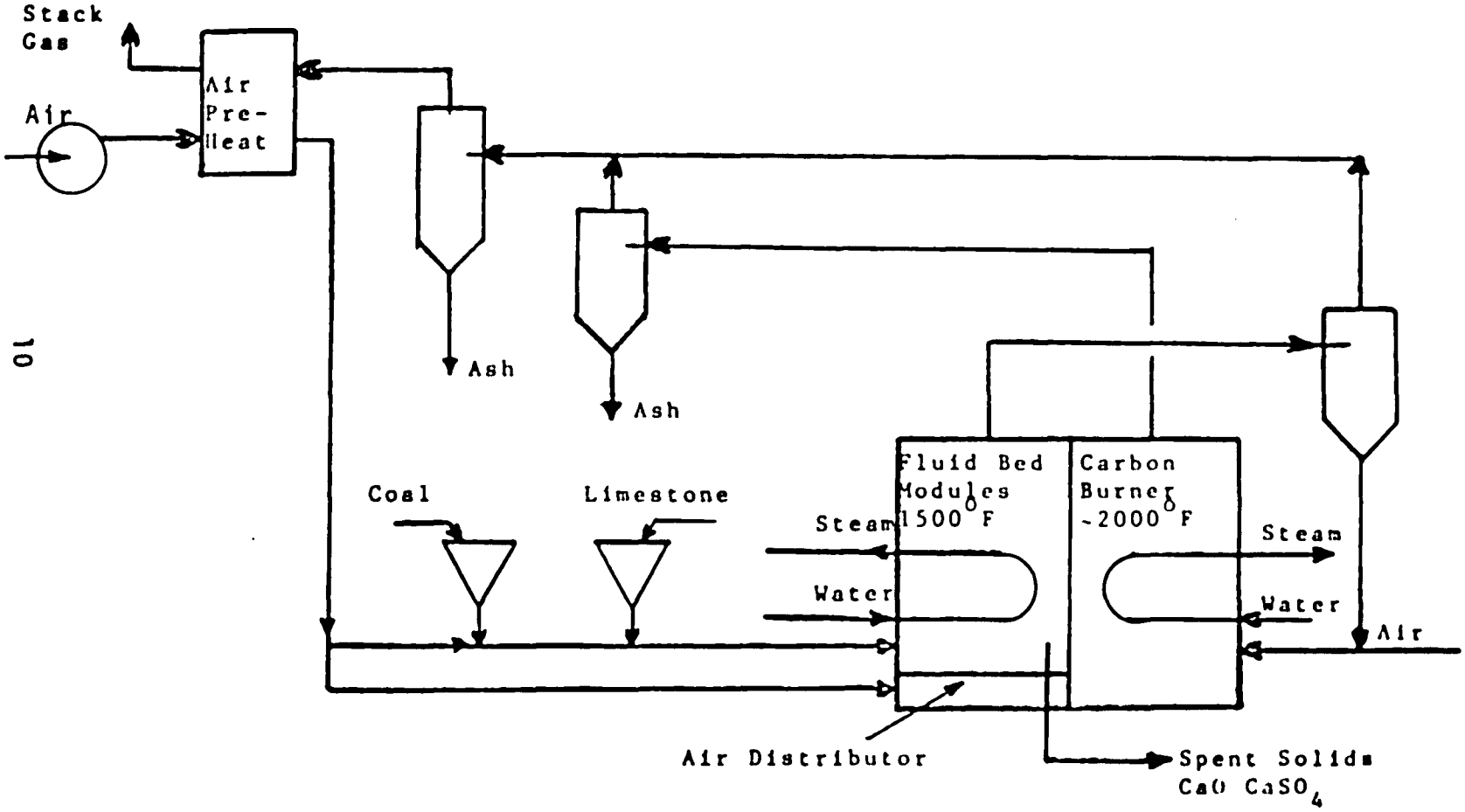

Fig. 4 Schematic Flow Diagram - Fluidized Bed Boiler and SO_2 Acceptor at 1 Atmosphere Pressure

ventional pulverized coal combustors. Fluidized bed boilers have been operated at atmospheric and high pressure conditions.

Figure 4 sketches the process flow. Air is preheated by exchange with stack gas. Part of the air conveys crushed coal (0 to 0.00635m) and limestone (8-10 mesh average) to the fluidized bed steam generator. The rest of the air enters through a distributor plate to support fluidization and combustion.

Spent limestone and sulfate with a low unburned coal content are removed for disposal.

Coal fines and ash are elutriated to a cyclone, recovered and combustion completed with 40 percent excess air in the carbon burn-up unit. There is also steam generation and/or superheating in this unit. Ash is recovered from the stack gas using electrostatic precipitators[2].

The fluidized combustor has several advantages:

- Efficient volumetric combustion reducing size and plant area needed and permitting shop fabrication.
- High heat exchange rates permitting low combustion temperatures.
- Reduced formation of nitrogen oxides.

- Relatively low excess air 5-10 percent.
- Coal may contain up to 60-70 percent moisture after bed is operating.
- Produces little or no alkali salts in flue gas.
- Coal rich in pyrites can be utilized.
- Handles high ash fuels, even with low softening temperatures.
- Full pulverization of coal not required.

Sulfur removal in the fluidized bed is accomplished by the reactions:

$$CaCo_3 \rightarrow CaO + CO_2$$

$$CaO + SO_2 + \frac{1}{2}O_2 \rightarrow CaSO_4$$

A big concern in sulfur removal is the degree of conversions of the CaO in a limestone particle. An important parameter in characterizing the amount of calcium required to achieve satisfactory sulfur removal is the Ca/S mole ratio. For a full stoichiometric ratio, all Ca going to sulfate, a thousand kilograms of 4 percent coal would require 97.5 Kg. of limestone to produce 122.47 Kg. of $CaSO_4$ for 90 percent sulfur removal[2]. Experiences indicate that only a fraction of this degree of conversion is accomplished at the desired fluidization state. The fluidized bed mentioned as an example in Figure 4 used a 6/1 Ca/S ration in the feed. At this ratio, a

thousand kilograms of 4 percent S coal would require 6 times as much carbonate or 585 Kg, and yields 273 Kg of Cao plus the 122.5 Kg of $CaSO_4$. Moreover, the Cao would react with water exothermically if used as land fill and the $Ca(OH)_2$ product is water soluble. Therefore, use of limestone with high Ca/S ratio give immense disposal problems, and chemical processing is required even for low Ca/S ration.

Ways might be found to separate and use the Cao or $Ca(OH)_2$ and/or $CaSO_4$ but a sizeable chemical plant would result.

Conventional fluidized beds have several disadvantages. In the fluidized bed combustor of the type studied by Pope Evans and Robins, Argonne National Laboratory, Exxon and others, the combustion air flows vertically upward through a horizontal distributor, fluidizing the bed material against the face of gravity. The coal combustion capacity of a combustion of this type, operating at a given temperature and pressure with bed material of a specified size, can be increased to a limited extent by increasing the superficial velocity of the fluidizing air. However, if the air velocity is increased too much, excessively high particle elutriation rates occur. Further increases of air flow rate can be

obtained only by increasing the bed cross sectional area. For large capacity power generation applications, this requires the use of a fluidized bed system consisting of a number of individual modules each of which is relatively large in size. Some possible consequences of this include difficulties with start up, coal and limestone feed, and bed mixing. Furthermore, the turndown capability of these systems is limited by reducing the air velocity nearly to minimum fluidization conditions and by reducing the operating temperature of the combustor. The thermal output of each combustor module can be varied over a ratio of approximately 2 to 1. Wider variations in output can be achieved by shutting down and starting up the individual fluid bed modules. Figure 5 shows several stages of fluidization occurring when small uniform particles (below 0.001m diameter) are subjected to an increasing gas velocity. First the particles in the bed vibrate, then they appear to move as a fluid. As the velocity is increased further, the gas forms larger and larger bubbles until slugging takes place. During slugging, clumps of particles act as a solid mass which moves ahead of a layer of gas. Thus giving very poor contacting conditions. Finally at higher velocities the particles are transported out of the bed. During each stage, the voidage in the bed in-

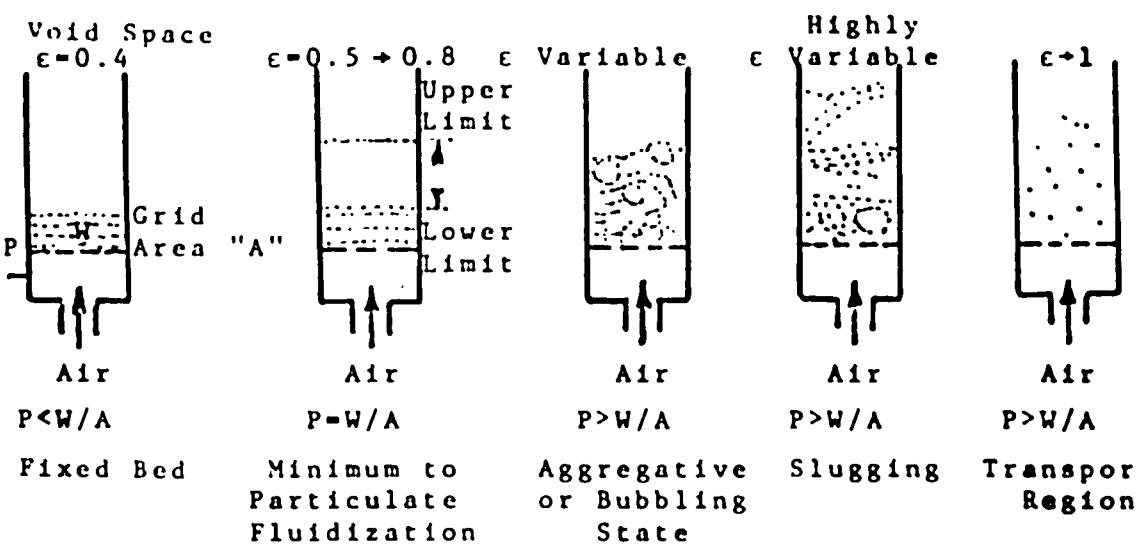

Fig. 5 Stages of Fluidization Occurring When Small Uniform Particles are Subjected to Increasing Gas Velocity in a Fluidized Bed (from Ref. 3)

creases, reducing the volumetric effectiveness of the equipment. For large, relatively low density particles, the transition from a fixed-bed condition to the slugging condition is almost immediate with increasing gas velocity. From the viewpoint of good gas to solid contact, this is clearly undesirable, since in the fixed-bed the gas flows through fixed channels with little particle movement, while in the slugging bed, most of the gas passes around the layers of particles without effective contact[3]. These drawbacks have limited the use of conventional fluidized beds.

B. Centrifugal Fluidization

The centrifugal fluidized combustor is a device cylindrical in shape, which rotates about its axis of symmetry (Figure 9). The centrifugal motion of the bed forces the bed particle into the annular region at the circumference of the combustor. Fluidizing air flows radially inward through the porous cylindrical surface of the device. The inward drag force of the fluidizing air on the bed material is balanced by the large radial accelerations caused by the centrifugal motion, permitting much larger air flow rates per volume of combustor than are possible with a conventional fluidized bed system operating against the force of gravity. This permits

more compact combustors. By varying the speed of rotation of the bed, the flow rate of air, and the bed temperature, it is possible to achieve considerable variation in system power output, providing the capability for operating over a wide range of part load conditions. In addition, the added flexibility due to bed rotation and the small size of the system should ease the problem of startup.

The centrifugal fluidized bed (CFB) overcomes the limitations of particle size through fluidization against a centrifugal force greater than the gravitational force. This has the effect of increasing the apparent density of the particles, allowing smooth, homogeneous fluidization. More importantly, smooth fluidization can be achieved at any desired gas velocity by varying the centrifugal force. Centrifugal force allows the bed operating parameters to be set independently of the physical properties of the material being heated. Consequently, one may operate on any of the regimes shown in Figure 5 at any given gas velocity.

The concept of a centrifugal fluidized bed is not new. Investigators at Brookhaven National Laboratory (BNL) performed experiments with 10^{-4}m and $5x10^{-4}$m glass beads in a 0.254m diameter bed and achieved fluidized

states at rotational speeds up to 209.44 rad/sec[4].

Experiments also were performed with $5x10^{-4}$m copper particles where fluidization was achieved at 73.3 rad/sec. Photographic records of the bed indicates stable fluidization at various rotational fields up to 560g's based on these results. Investigators at BNL proposed using a centrifugal fluidized bed coal liquefaction[4]. Experiments on the use of a rotating fluidized bed as a particle filter have been reported[4]. In addition, investigations on this system are being done for food drying applications[3].

Experimental investigations on this system have been under way at Lehigh University since 1976. The present research involves studies of bed startup, minimum fluidization and particle elutriation.

The objectives of this study are to demonstrate the capability to operate a centrifugal fluidized bed with continuous feed and removal of bed material and to obtain quantitative information on the effects of the additions of solids on bed characteristics.

II. APPARATUS AND INSTRUMENTATION

A. Air Supply

Air is supplied by two positive displacement compressors each nominally rated at 0.234SCMS and 6.9x 10^5Pa. Air leaving the compressors flows through an oil separator to an air storage tank and finally to the fluidized bed laboratory. After passing through a globe valve, it passes through a section of pipe densely packed with commercial grade steel wool which reduces the pressure and muffs the flow noise. After the muffles, the velocity profile is developed hydrodynamically in a 2.5m section of (0.1016m I.D.) pipe. The air then flows into a section with a calibrated (0.003175m diameter) pitot-static probe for air flow rate measurement. Probe dynamic pressure is indicated on a differential vertical inclined manometer rated at a maximum of 0.254m of water. This system is used for all flow rate measurements and has a range from 0.04 to 0.448SCMS.

A manifold with two (0.102m diameter) equal size outlets distributes the air flow to the fluidized bed apparatus through flexible hoses which connect the manifold holes to the inlet air plenum of the apparatus. The system is also designed with an (0.0508m diameter) air line connected to the lower part of solids discharge plenum to control the rate of discharged solids. This

control line was not used during the experiments described in this thesis.

B. Feed System

The feed system consists of a Petrocarb ABC injector, an injection hose and rod, and solids distributor plate in the rotating chamber. These are described below.

The Petrocarb ABC injector system (Figure 6) is designed to inject particles from a pressurized tank into an air line, through which the particles are conveyed pneumatically into the test section. The pressurized tank, which is the heart of this system, was loaded up to 100 Kgm of particles which we used in experiments, and is rated at a pressure of 413685Pa above atmosphere. The external parts of the ABC injector consist of the gas control equipment, mixing assembly, filling valve, exhaust and relief valve. An air supply line, after passing through a pressure regulator, is connected to a small rotameter which can measure air flow rates up to 0.001525SCMS under 275790Pa above atmosphere. It then is divided into two branches, one of which goes to the tank pressure regulator, tank pressure gauge, tank pressurizing valve, and then pressurizes the injector tank. The other air stream, which flows through several valves,

gauges and a regulator, provides conveying air to carry the injected solids to the fluidized bed.

Figure 6 shows the entire system, including the pressure tank. At the top of the pressure tank are an exhaust valve, a pressure relief valve and filling valve. Installed at the bottom of the pressure tank are a valve to control solids flow rate (0.00635m), a quick disconnect coupling, and an (0.003175m) orifice (Figure 7).

Solids feed rate is controlled by regulating the tank pressure. Calibration data for the system show only a very small effect of conveying air on solids flow rate. The tank pressure is controlled by adjusting the tank pressure regulators, while the conveying air flow is controlled by adjusting the control valve until the desired flow rate is indicated on the rotameter. The tank is loaded from the top by depressurizing the tank and then opening the fill valve.

For starting up the feed system, the following procedures were used: (i) pressurize the tank, (ii) adjust the conveying air, (iii) open the solids feed valve.

A flexible (0.0095m I.D.) metal hose was used as the injection hose to convey the particles from the pressure tank to the fluidized bed. It is connected at the bottom

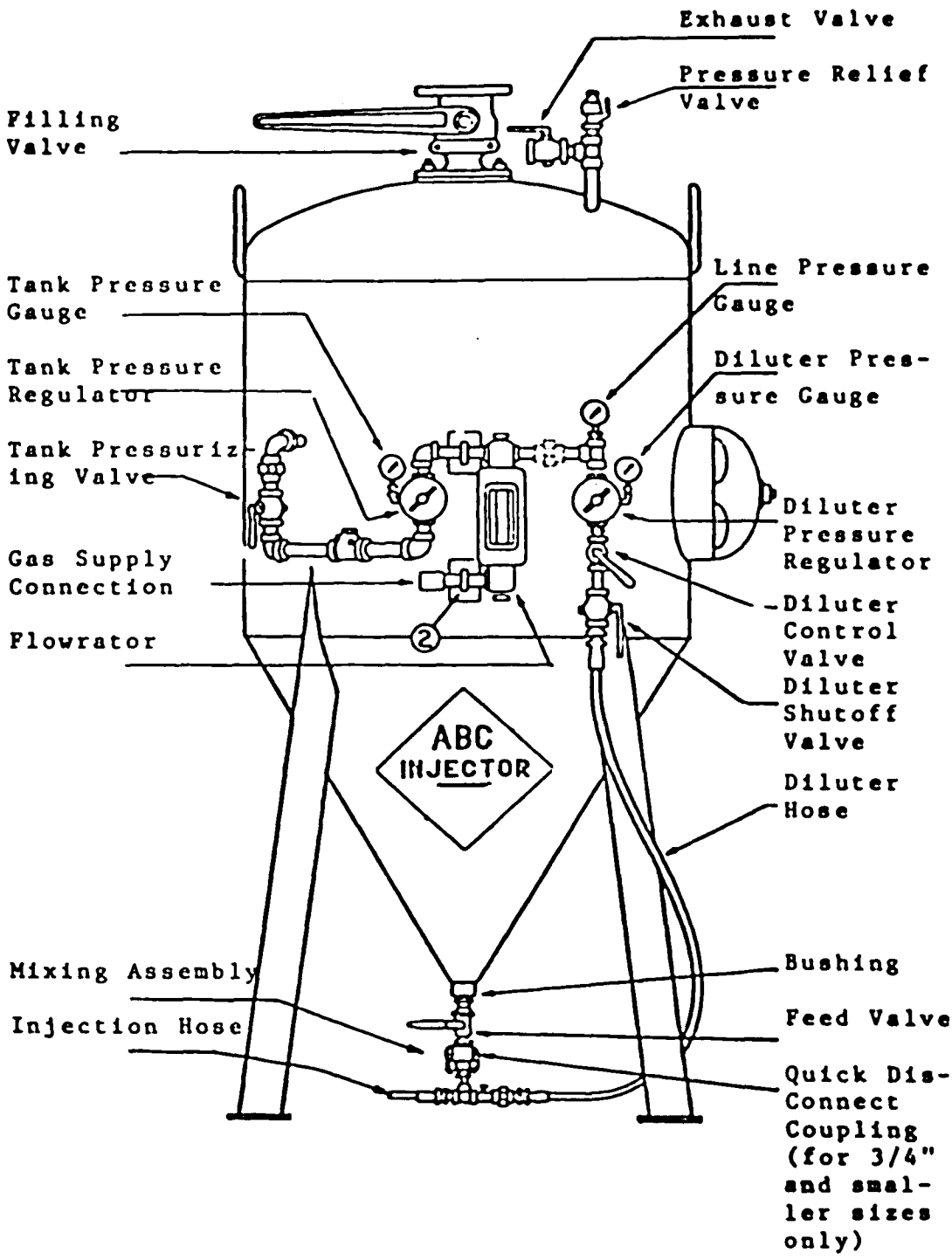

Fig. 6 ABC Injector

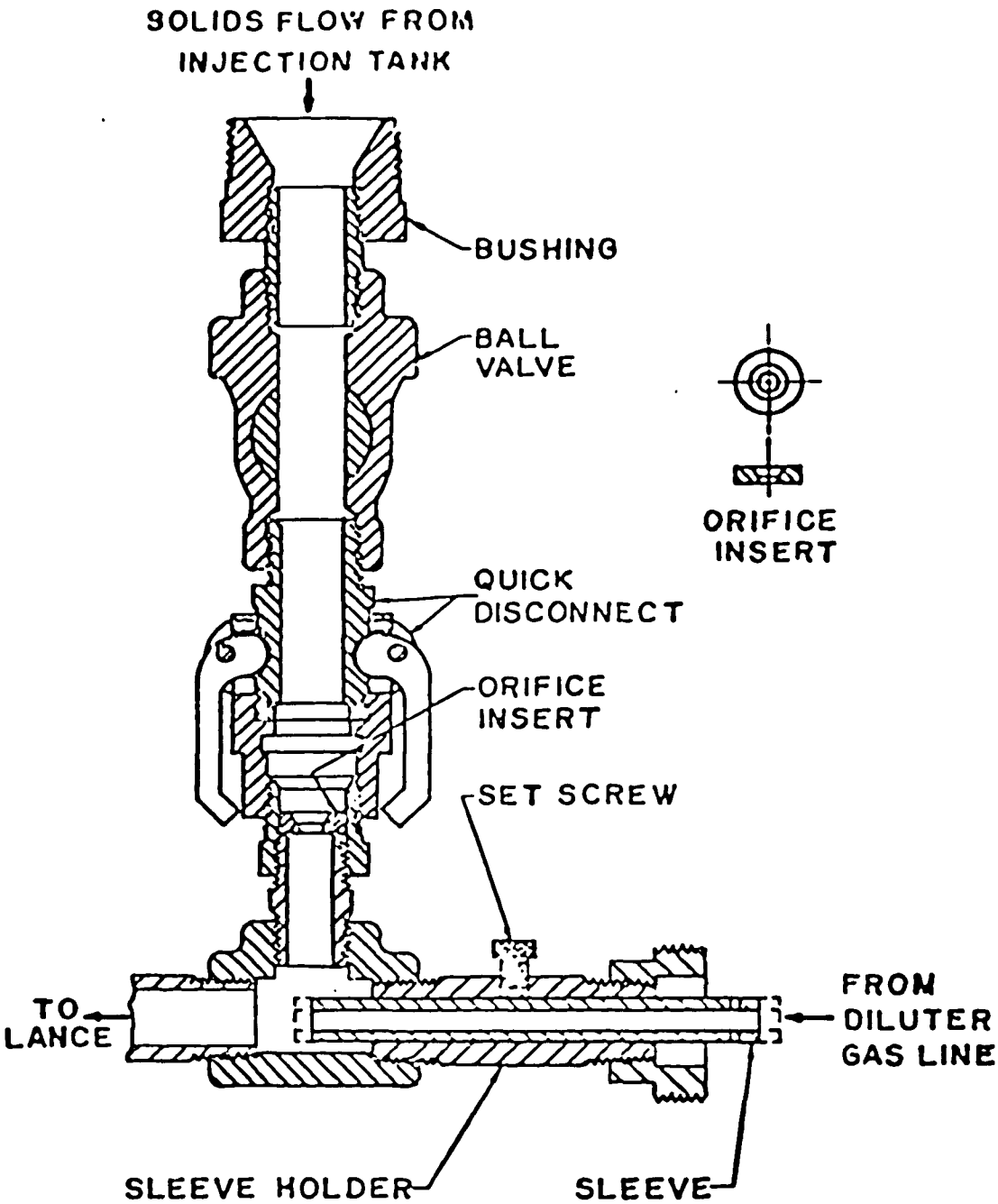

Fig. 7 Cross Section of Mixing Valve Assembly

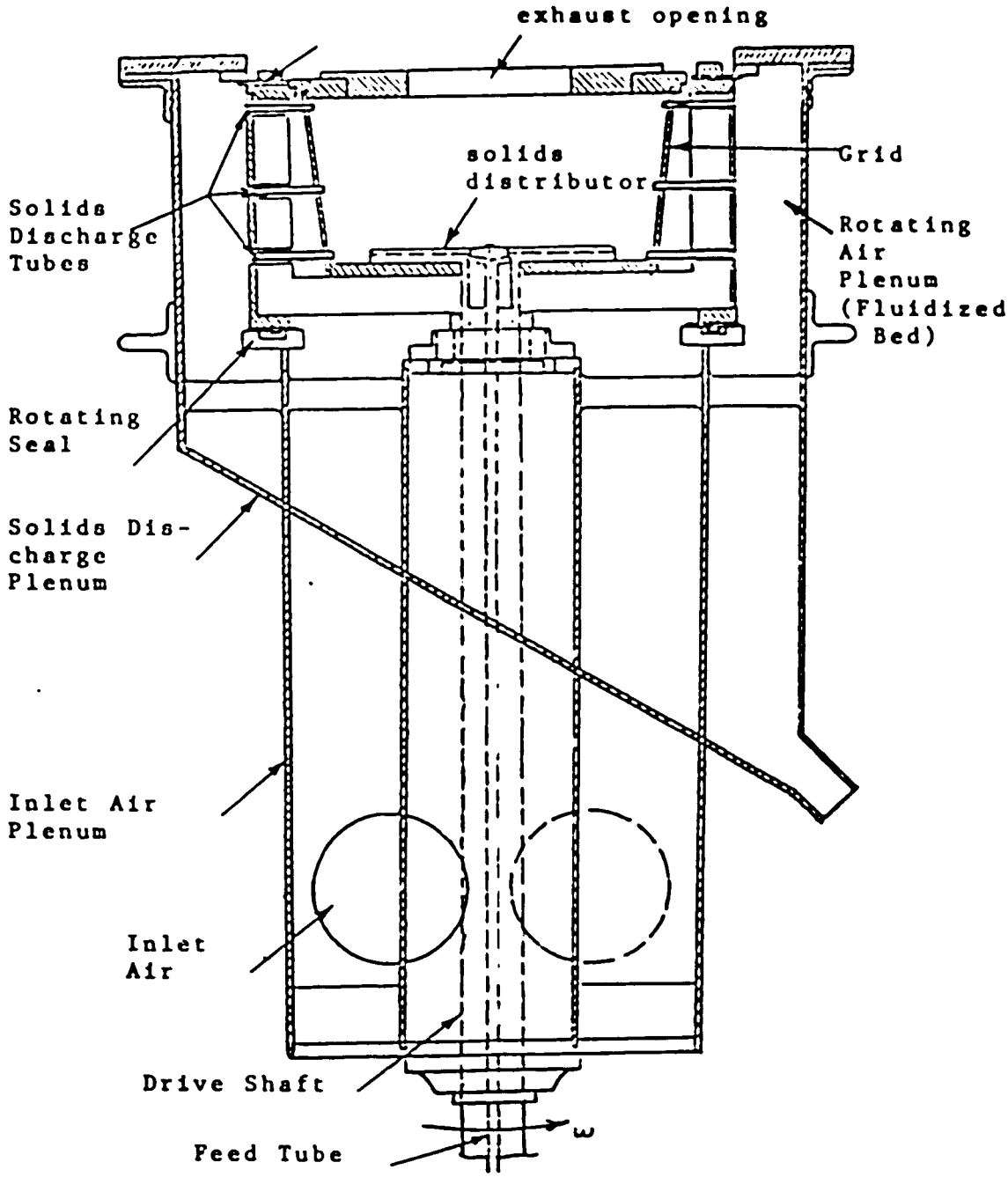

Fig. 8 Cross Section of Apparatus

of the test section (Figure 8) to a 0.009525m I.D. copper tube. The copper feed tube, designed not to rotate during bed operation, coupled to a 0.23m I.D. circular plexiglass plate in the bottom of the fluidized bed. Injected solids are conveyed vertically upward through the feed tube and are forced radially outward to the bed region through two channels in the distributor plate. Feed system specifications are given in Table 5.

C. Apparatus

The test section consists of a rotating air plenum (fluidized bed), an inlet air plenum, a solids discharge plenum, a discharge bin and load cells, and a motor and rotating shaft.

The fluidized bed shown in Figure 9 is actually the heart of the system. An important part of the fluidized chamber is the grid through which the fluidizing air from the inlet air plenum passes to fluidized the particles. If the grid is not designed properly, the apparatus may not achieve a stable fluidized state. Based on results from an earlier study on the influence of grid design on bed performance, the grid was fabricated from perforated steel sheet metal with 50 percent open area[5]. The grid has the shape of a truncated cone. The seam of

the rolled metal sheet was butt-welded, ground smooth, and was covered on the inside periphery with fine mesh stainless steel cloth. Great care was taken to insure that the wire cloth was in close contact with the perforated steel frame throughout. The wire cloth screen is attached to the frame by means of circumferential beads of silver solder. Contact of the screen and the frame is insured by stitching the screen to the frame at appropriate locations around the periphery.

To increase the resistance of the grid to air flow, a layer of canvas-like cloth is stitched around the outside of the frame, after being stretched tight to insure close contact of the cloth with the frame everywhere. The cloth is secured at the top and the bottom using very thin pieces of tape to prevent bypass of fluidizing air around the cloth at the boundaries. Figure 10 shows a cross-section of the grid. As shown in Figure 9, the grid assembly at the bottom is held by a solid plate and at the top is sealed into the grooves which have been made for this purpose. The dimensions of the grid are given in Table 3 (Apparatus Specifications).

Air flows into the apparatus through two (0.1524m I.D.) openings (Figure 11) and then through the grid to fluidized the particles. The top end wall of the flui-

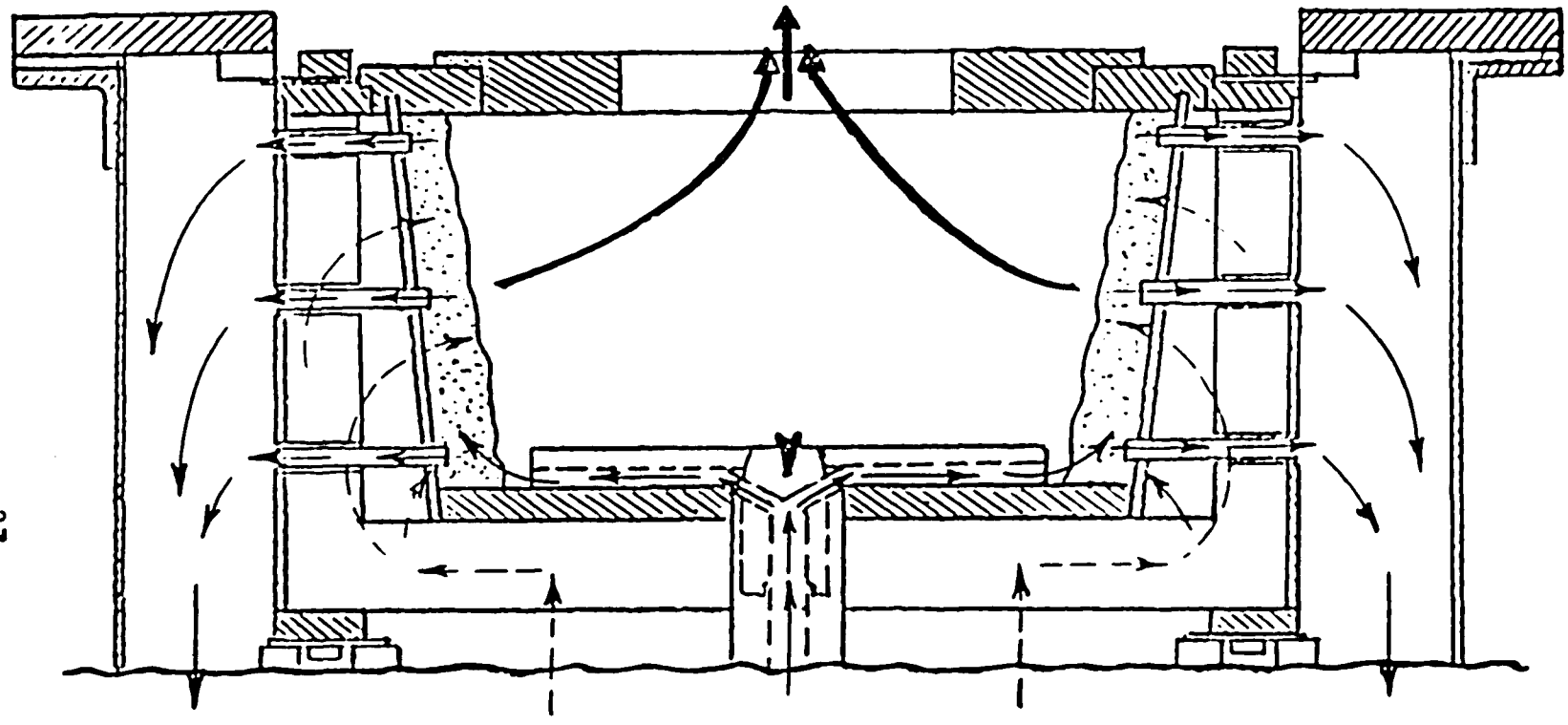

Fig. 9 Sketch of Fluidized Bed

Solids

Air

Exhaust Products

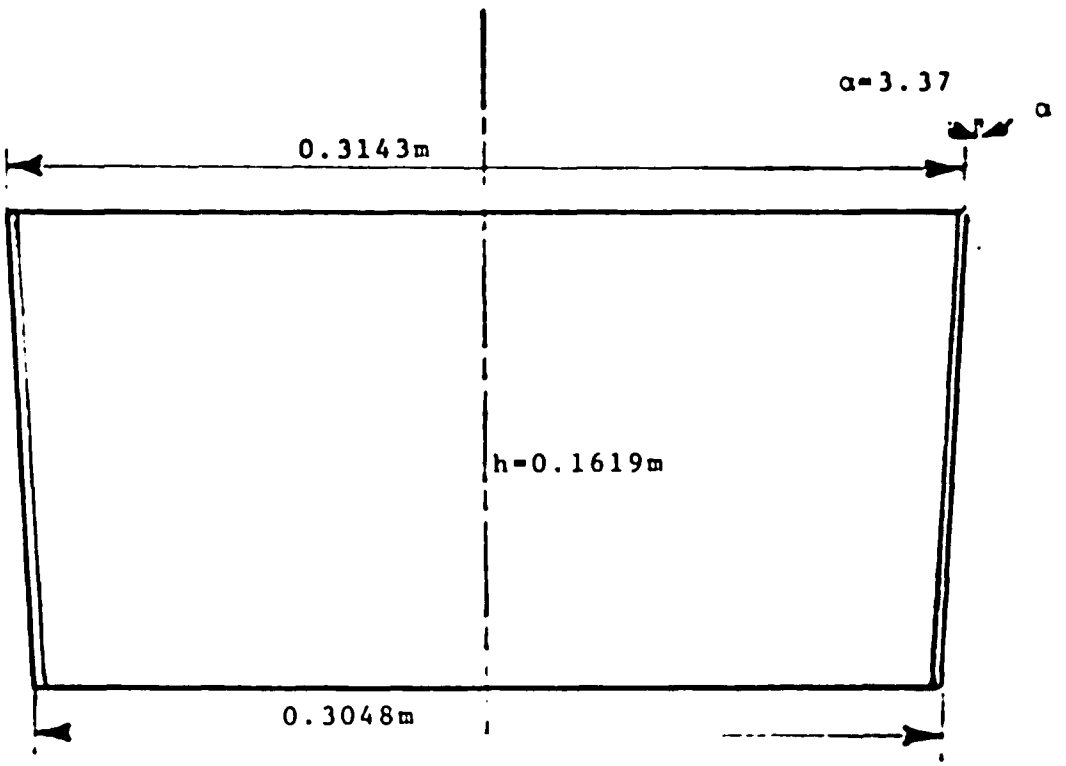

(1) 22 G perforated steel frame, 50% open area
a

(2) Stainless steel screen attached inside with solder beads top and bottom (U.S. sieve 200 mesh)

(3) Cloth stitched to outside of grid

Fig. 10 Cross Section of Grid

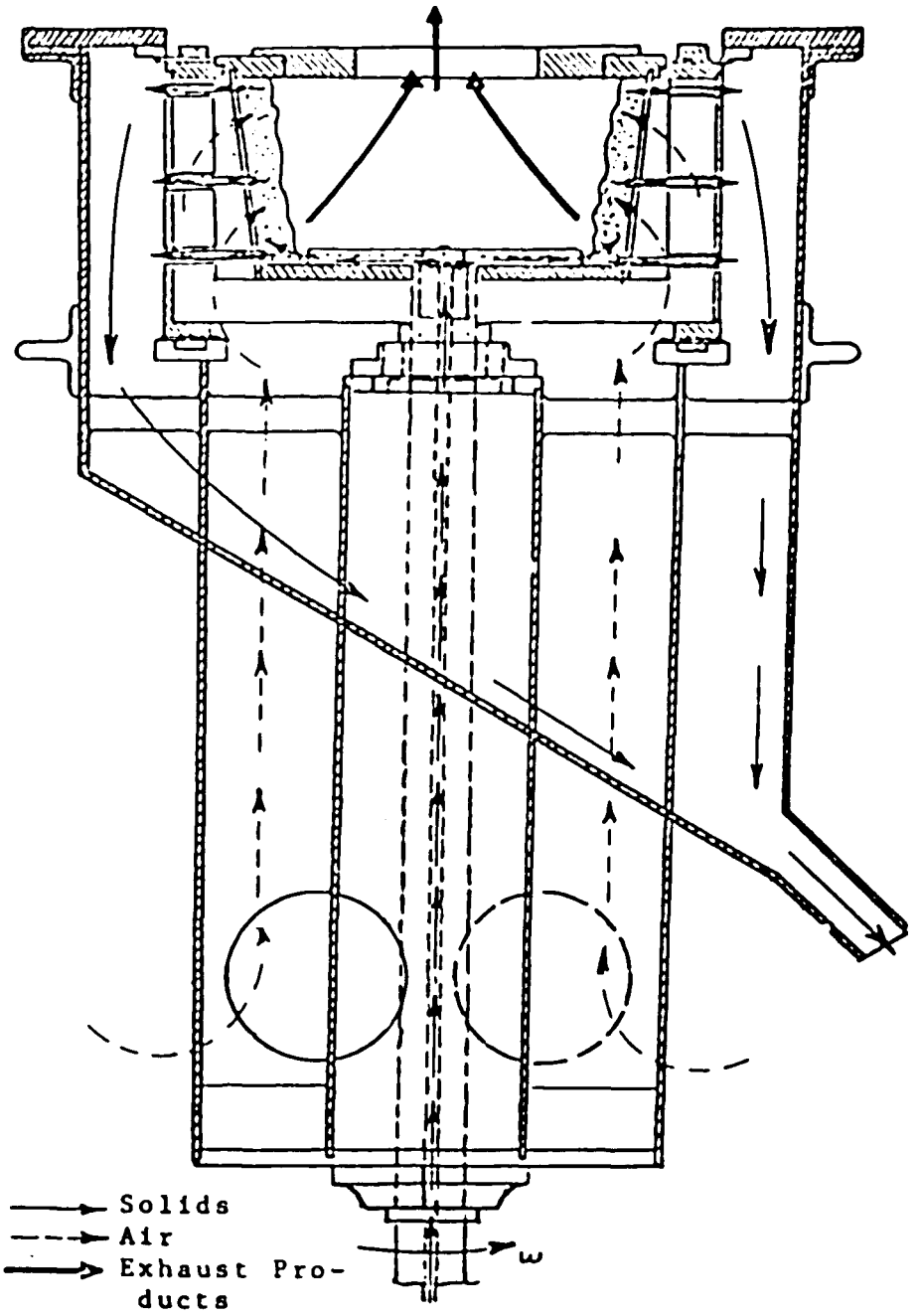

Fig. 11 Cross Section of Apparatus
Solids & Air Directions

dized bed has a 0.1524m diameter opening for discharge of air, and is fabricated from plexiglass for flow visualization.

Solids are discharged from the rotating bed through six small (0.009525m I.D.) tubes, passing through the grid (Figure 9) to the solids discharge plenum. These tubes can be changed easily for studies of the effects of length and diameter of discharge tubes on the solids discharge rate.

The solids discharge plenum is the stationary outer cylinder shown in Figure 8. The bottom of the plenum has a sharp slope to facilitate solids flow. From the discharge plenum, particles drain through a 0.0508m I.D. flexible hose into the discharge bin. The frame of the apparatus is fixed to the body of the cylinder by two bearings, which make it possible to incline the apparatus away from the vertical position.

Pressure taps are used to measure the pressures of the inlet air plenum and the solids discharge plenum. These taps are connected by PVC tubing to a 1.5m vertical manometer board.

The discharge bin is a closed vertical cylinder which is connected to the solids discharge plenum by a flexible

hose. The bin is supported at the bottom by three load cells (which are discussed later) to indicate the weight of discharged particles at any instant of time. A cover plate attached to the side of the bin can be removed to empty solids from the bin. The dimensions of this bin are given in Table 3.

A 0.5Hp, (DC) variable speed motor is used to rotate the system. The motor is attached to the rigid frame and is belt connected to the drive shaft. The angular velocity of the test section was measured using a General Radio Company "strobotac" stroboscope type 1531-A.

One circular teflon seal is used to separate the rotating air plenum and inlet air plenum, and a second circular teflon seal separates the rotating air plenum and solids discharge plenum.

Special consideration also was made to minimize vibration during rotation. The steel frame of the apparatus is bolted to the concrete floor.

The weight of the discharged particles was recorded continuously by load cells, mounted at the bottom of the discharge bin. The load cells are of cylindrical ring design, each with four strain gauges (Figure 12a).

These load cells are connected in parallel to each other (Figure 12b) and are excited with a 10V(DC) power supply. The readout device is a digital volt meter model 8040A with 200mv range $\pm$ (0.05 percent of reading + three digits) and 2V through 1100V range $\pm$ (0.05 percent of reading + two digits). Table 2 gives the specifications of the strain gauges used in the load cells.

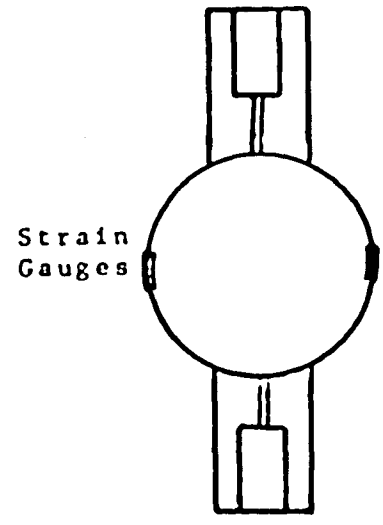

(a) Sketch of a Load Cell

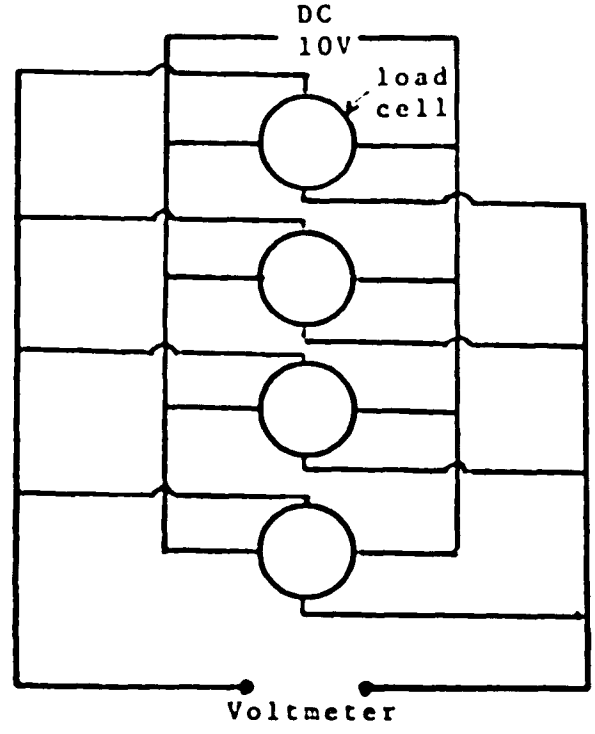

(b) Connection of Load Cells in Parallel

Fig. 12 Load Cells

TABLE 2 - STRAIN GAUGE SPECIFICATIONS

Model, EA-06-062AP-120 Micro-Measurement Products

Resistance in OHMS 120+0.3 percent

Gauge factor at 75°F 2.045+0.5 percent

Strain limit 5 percent for gauge length (0.0032m) and larger, and approximately 3 percent for gauge lengths under (0.0032m)

TABLE 3 - APPARATUS SPECIFICATIONS

Description	
Diameter of exhaust opening	0.15m
Outside diameter of discharge plenum	0.6m
Outside diameter of inlet air plenum	0.395m
Inside diameter of solids discharge tubes	0.009525m
Distributor plate diameter	0.23m
Grid height	0.1619m
Grid radius at bottom	0.3048m
Grid radius at top	0.3143m
Grid taper angle	3.37°
Inlet air diameter	0.1016m
Outside diameter of drive shaft	0.05556m
Outside diameter of discharge bin	0.455m
Height of discharge bin	0.455m
Height of load cell	0.068m
Height of test section	1.105m
Motor type DC	0.5HP

TABLE 4 - RANGE OF OPERATING VARIABLES

Description	
Maximum angular velocity	48.17 rad/sec
Maximum measurable air flow rate	0.448 SCMS
Minimum measurable air flow rate	0.04 SCMS
Maximum measurable plenum pressure	18000 Pa above atm.
Minimum measurable plenum pressure	5 Pa above atm.
Maximum calibrated weight by load cells	22.7 Kg.

TABLE 5 - FEED SYSTEM SPECIFICATIONS

Description	
Maximum solids loaded in tank	100 Kg.
Maximum allowable pressure in tank	413685 Pa above atm.
Maximum allowable temperature	93.3°C
Maximum measurable conveying air	0.001525 SCMS
Air line pressure	275790 Pa above atm.
Average particle size used	410×10^{-6}m
Orifice diameter	0.003175m
Feed valve	0.00635m
Inside diameter of injection hose	0.009525m
Fill valve	With electric control

D. Instruments Calibration

1. Load Cell

As was stated, the load cells were connected in parallel to each other (Figure 12), and the discharge rates were recorded continuously. They were placed at the bottom of the discharge bin and calibration was performed by loading standard weights on the discharge bins. These load cells were excited by 10V DC power supply and the readout system was a digital voltmeter which was described before. Figure 13 shows the calibration chart for these load cells.

2. Air Flow Rate

The shape of the velocity profile in the main air line (0.102 m I.D) was determined by traversing the pipes diameter with a pitot-static probe and recording the kinetic pressures at 0.003175 m intervals.

The volumetric air flow rate was found by integrating the velocity profile over the pipe cross-section in the horizontal and vertical directions. This procedure was repeated for several different air flow rates. The basic equations for this calibration are:

$$V = \frac{\sqrt{2P_d}}{\sqrt{\rho_f}} \text{ and } m^o = \rho_f \sum_{n=1} V_n \Delta A_n$$

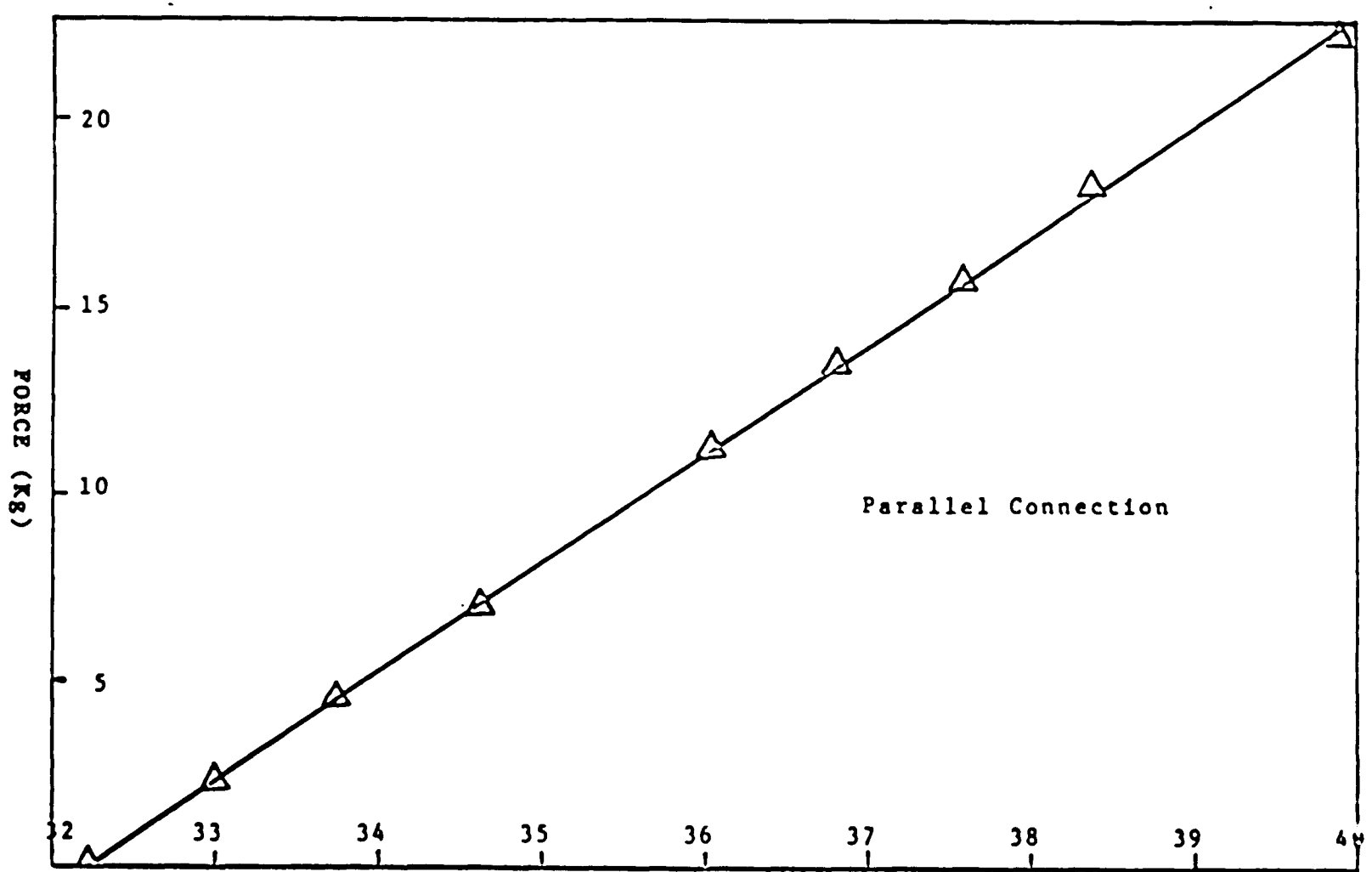

Fig. 13 Calibration Data for Load Cells

By considering the above procedures a plot was made of the squareroot of centerline kinetic pressure versus volumetric flow rate (Figure 14). The following linear relationship was obtained:

Volumetric air flow rate:

$$(m^3/sec) = 0.009695\sqrt{(P_d)_{\ell}}$$

where $(P_d)_{\ell}$ is the kinetic pressure at the centerline of the pipe measured in (Pa).

3. *Feed System*

The feed system was calibrated with the ratio of the flow rate of fluidizing air to flow rate of solids of the order of 40/1. The superficial air velocity inside the injection hose (0.00952 m I.D.) was set equal to 15.24 m/sec. During the calibration, the pneumatic flow tube was connected to a cyclone and the solids discharge from the cyclone was weighed to determine solids flow rate. In this calibration and also during all the experiments the main regulator was set on 275790 Pa above atmosphere.

The calibration was performed for glass bead particles with $\overline{dp} = 410 \times 10^{-6}$m and the results of the calibration are shown in Figures 15 and 16. As is shown in Figure 15, over the range tested, the solids

feed rates are almost independent of flow rate of conveying air. In Figure 16, it is shown that solids feed rate varies nearly linearly with tank pressure.

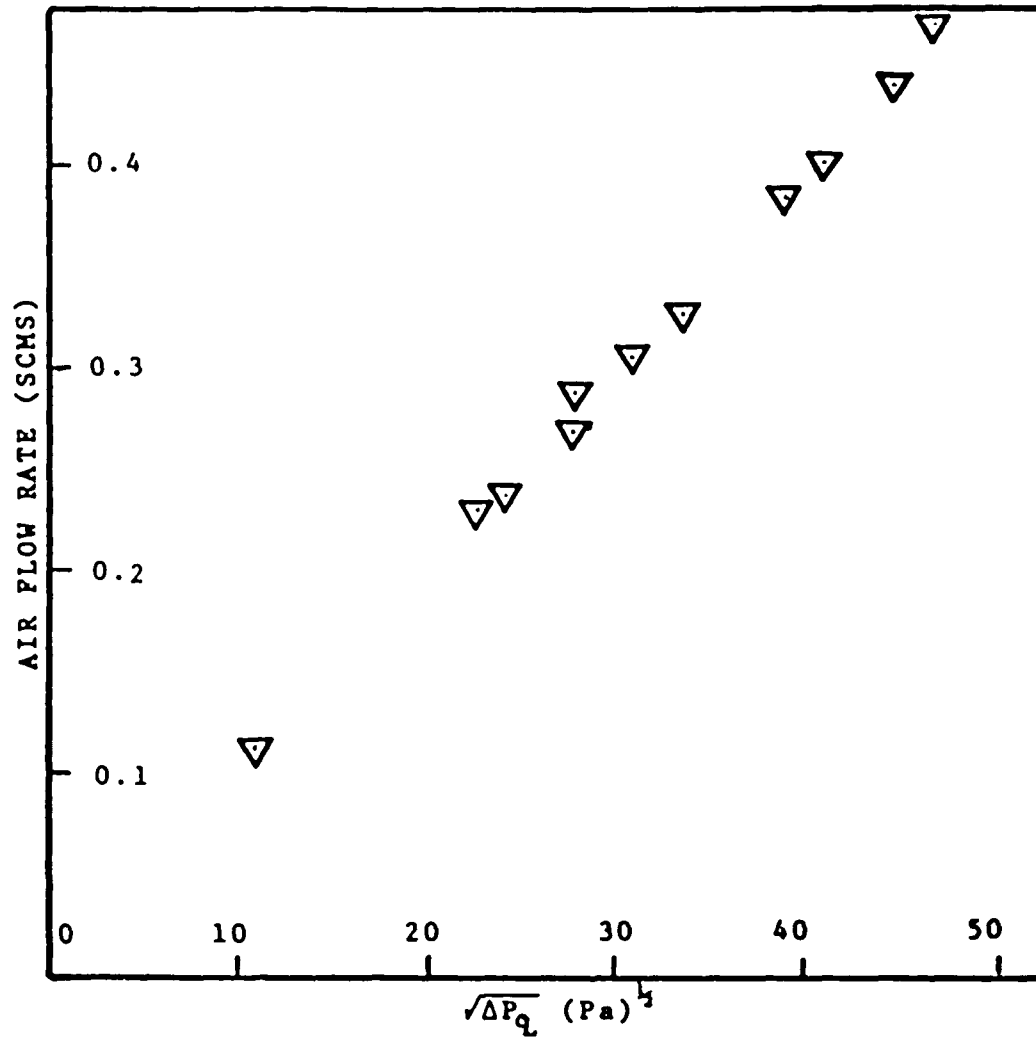

Fig. 14 Calibration Data for Air Flow Rate

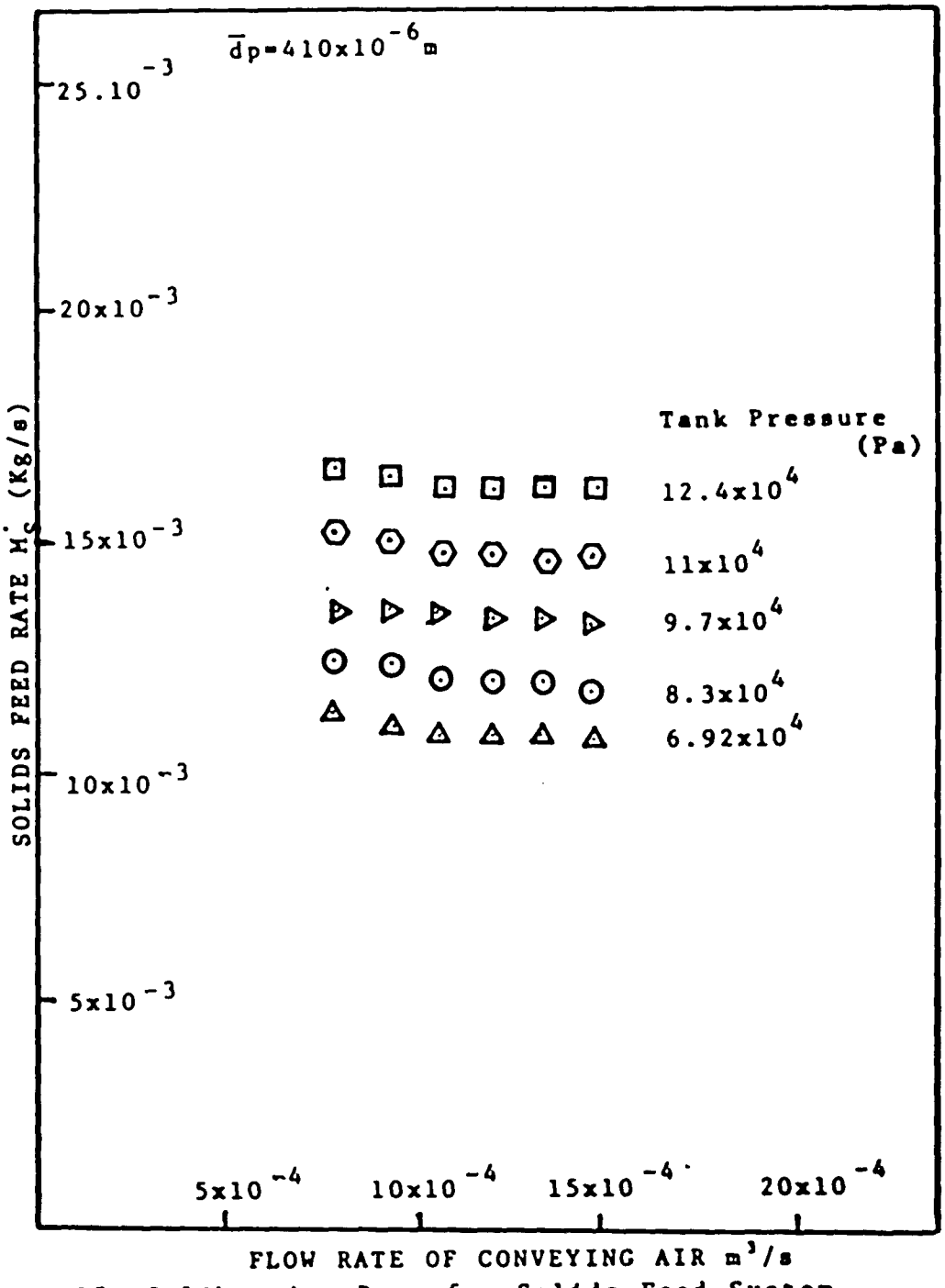

Fig. 15 Calibration Data for Solids Feed System

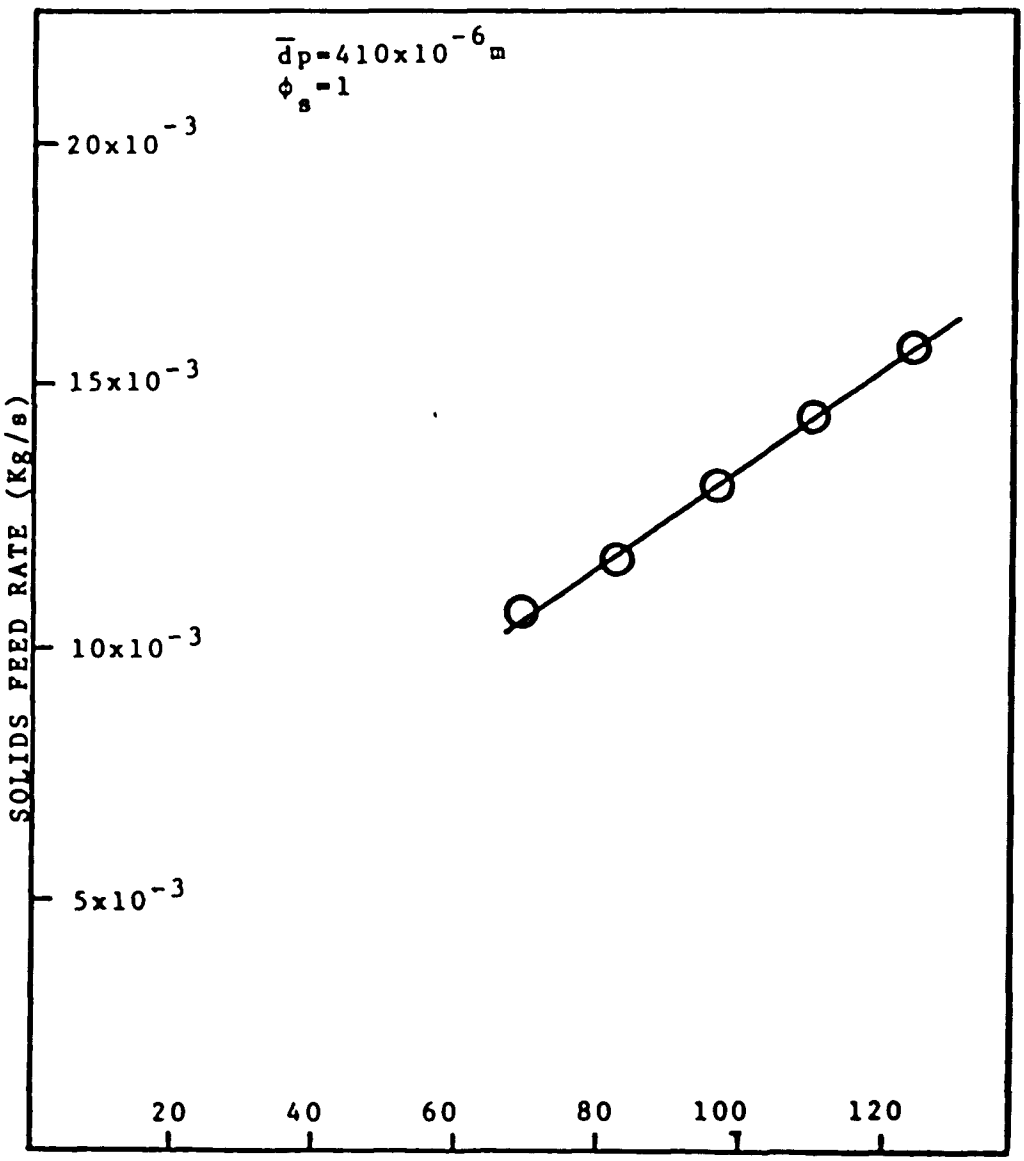

Fig. 16 Calibration Data for Solids Feed System

III. BATCH EXPERIMENTS

A. Review of the Theory

In this chapter a theoretical analysis of the rotating fluidized bed developed by references [4,5,6] is described and compared with experimental results on bed pressure drop. Martin [5] obtained an expression for the shape of the free surface of the bed by assuming the bed behaves as a liquid in rigid body rotation. For the case where the bed covers the entire grid (Figure B-1) he found:

$$x_1 = \frac{\omega^2}{2gH}\left(\frac{H^3}{3}\tan^2\alpha - H^2 r_{o2}\tan\alpha + H r_{o2}^2 - \frac{m}{\pi\rho_s(1-\varepsilon)} - \frac{gH^2}{\omega^2}\right) \tag{3.1}$$

$$r_i = \frac{\sqrt{2g(x_1+Z)}}{\omega} \tag{3.2}$$

$$r_o = (x_1+Z)\tan\alpha + r_{o2} - (x_1+H)\tan\alpha \tag{3.3}$$

For the cases where the grid is partially exposed (Figure B-2) he obtained:

$$x_1 = \frac{\omega^2}{2g}\left(h'^2\tan^2\alpha + 2r_{o1}h'\tan\alpha + r_{o1}^2 - \frac{2gh'}{\omega^2}\right) \tag{3.4}$$

and

$$\frac{h'^3}{3}\tan^2\alpha + r_{o1}h'^2\tan\alpha + r_{o1}^2h' - \frac{gh'}{\omega^2}(h' - 2gx_1) = \frac{m}{\pi\rho_s(1-\varepsilon)} \tag{3.5}$$

by solving equations (3.4) and (3.5), x_1 and h' are found.

Discussing the velocity profile and shape of the bed are presented in Appendices A and B. Levy, et al obtained equations for bed pressure drop and minimum fluidization velocity [4]. With a uniform tangential velocity profile, the pressure drop through the fluidized bed is:

$$P(r_o) - P(r_i) = \Delta P_B = (\rho_s - \rho_f)(1 - \varepsilon) r_o^2 \omega^2 \ell n \frac{r_o}{r_i} \quad (3.6)$$

With rigid body rotation, the bed pressure drop is calculated from the equation:

$$P(r_o) - P(r_i) = (\rho_s - \rho_f)(1 - \varepsilon) \frac{\omega^2 r_o^2}{2} \left[1 - \left(\frac{r_i}{r_o}\right)^2\right] \quad (3.7)$$

The packed bed pressure drop for the centrifugal bed is found to be (Ergun equation):

$$\Delta P_{BP} = \frac{150(1-\varepsilon)^2 \mu \ell n(\frac{r_o}{r_i})}{\varepsilon^3(\phi_s d_p)^2(2\pi\rho_f)} \dot{m}_H + \frac{1.75(1-\varepsilon)}{\varepsilon^3 \phi_s d_p \pi^2 (4\rho_f)} \left(\frac{1}{r_i} - \frac{1}{r_o}\right) \dot{m}_H^2 \quad (3.8)$$

where

$\dot{m}_H$ = mass flow rate per unit height

L = depth of bed

ϕ_s = sphericity

d_p = diameter of sphere having volume of particles which could be replaced by $\bar{d}_p$

Equating the expression for packed bed pressure drop to the fluidized bed pressure drop, the superficial velocity of the gas at minimum fluidization was determined by Levy and Martin [7]. Expressed in terms of particles Reynolds number and Galileo number this correlation is:

$$Ga = \frac{300(1-\varepsilon)\ln(\frac{r_o}{r_i})}{\varepsilon^3\phi_s^2[1-(\frac{r_i}{r_o})^2]} Re_{MF} + \frac{3.5(\frac{r_o}{r_i}) - 3.5}{\varepsilon^3\phi_s[1-(\frac{r_i}{r_o})^2]} Re_{MF}^2 \qquad (3.9)$$

where

$$Ga = \frac{\rho_f(\rho_s-\rho_f)\omega^2 r_o d_p^3}{\mu^2} \quad , \quad Re_{MF} = \frac{\rho_f U_{MF} d_p}{\mu}$$

In this case also the mean particle size $\bar{d}_p$ is used with a bed containing a wide particle size distribution.

Martin [5] developed a computerized procedure which accounts for vertical variations in bed thickness in computing minimum fluidization and bed pressure drop. This analysis, described in more detail in Appendix C, is compared in this thesis to results obtained during the batch experiments.

Void fraction is defined as:

$$\varepsilon = \frac{\text{volume of void}}{\text{total volume}}$$

In the packed regime the bed pressure drop is an extremely strong function of void fraction. However the void fraction has no effect on bed pressure drop at

fluidization condition. It does influence the transition region and the calculated point of minimum fluidization. Figure 17 shows this effect with results taken from Martin's computer analysis.

B. Experimental Procedure

1. Measurement of Mean Particle Size

Technical quality glass spheres were used for the experiments and particle size distributions were determined by sieving. The mean particle size $\bar{d}_p$ was calculated as follows:

x_i = weight fraction of sample within a specified size range i

d_{p_i} = arithmetic average of particle minimum and maximum diameter in size range i

$$\bar{d}_p = \frac{1}{\sum_{\text{all } i} \left(\frac{x_i}{d_{p_i}}\right)}$$

For example, consider the following size distributions.

U.S. Sieve No.	Wt. % Passed
35	91.3
40	8.69
45	0.01

Diameter Range x 10^6m	d_{p_i}	x_i	$(x/d_p)_i$
0 - 354	177	0.0001	0.565×10^{-6}
354 - 380	367	0.0869	236.78×10^{-6}
380 - 450	415	0.913	2200×10^{-6}

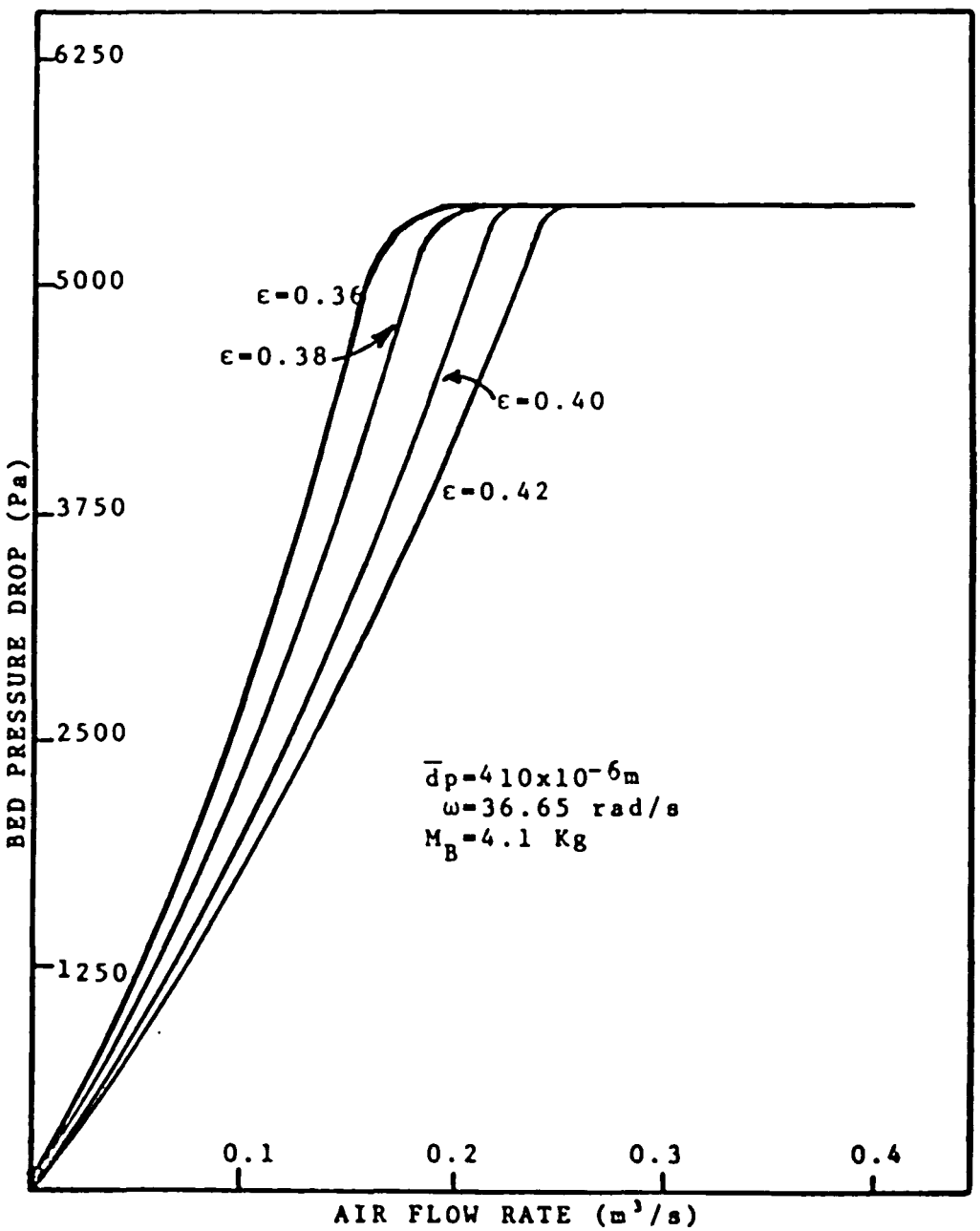

Fig. 17 Theoretical Results on Effect of Void Fraction on Pressure Drop

$$d_p = 410.3 \times 10^{-6} m$$

2. Grid Pressure Drop

In order to measure the grid pressure drop, the following procedures were followed: (i) The rotating plenum was vacuum cleaned completely, (ii) The pressure taps were connected to the 1.5m vertical manometer board, (iii) The motor was started up and the angular velocity of the drive shaft was adjusted to match the desired strokoscope frequency, (iv) The air supply valve was opened slowly from a very low air flow rate to the highest possible air flow rate and at each air flow rate the pressure was recorded, (v) These processes were repeated for several bed angular velocities.

Figure 18 shows one series of these tests for different angular velocities. Because of change in environmental conditions such as humidity during the period when the experiments are performed, the particles gradually stick to the body of the grid, and therefore the grid pressure drop does not remain constant during the period of experiments. Also particles might fracture during use and small fragments could plug up the grid, increasing grid flow resistance. For these reasons, at the beginning of each test the grid pressure drop was measured.

Figure 19 compares the grid pressure drop for two different dates.

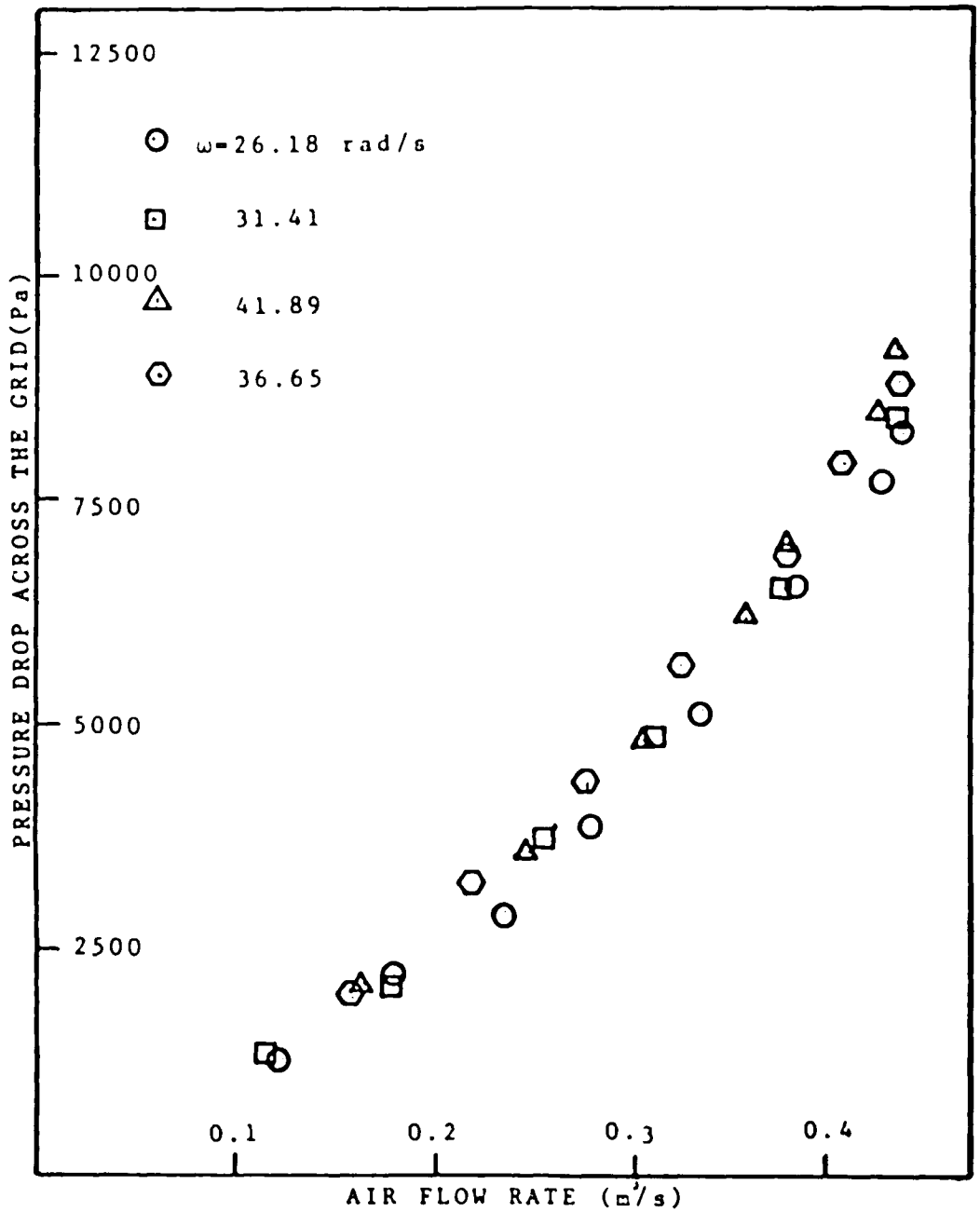

Fig. 18 Calibration Data for Grid

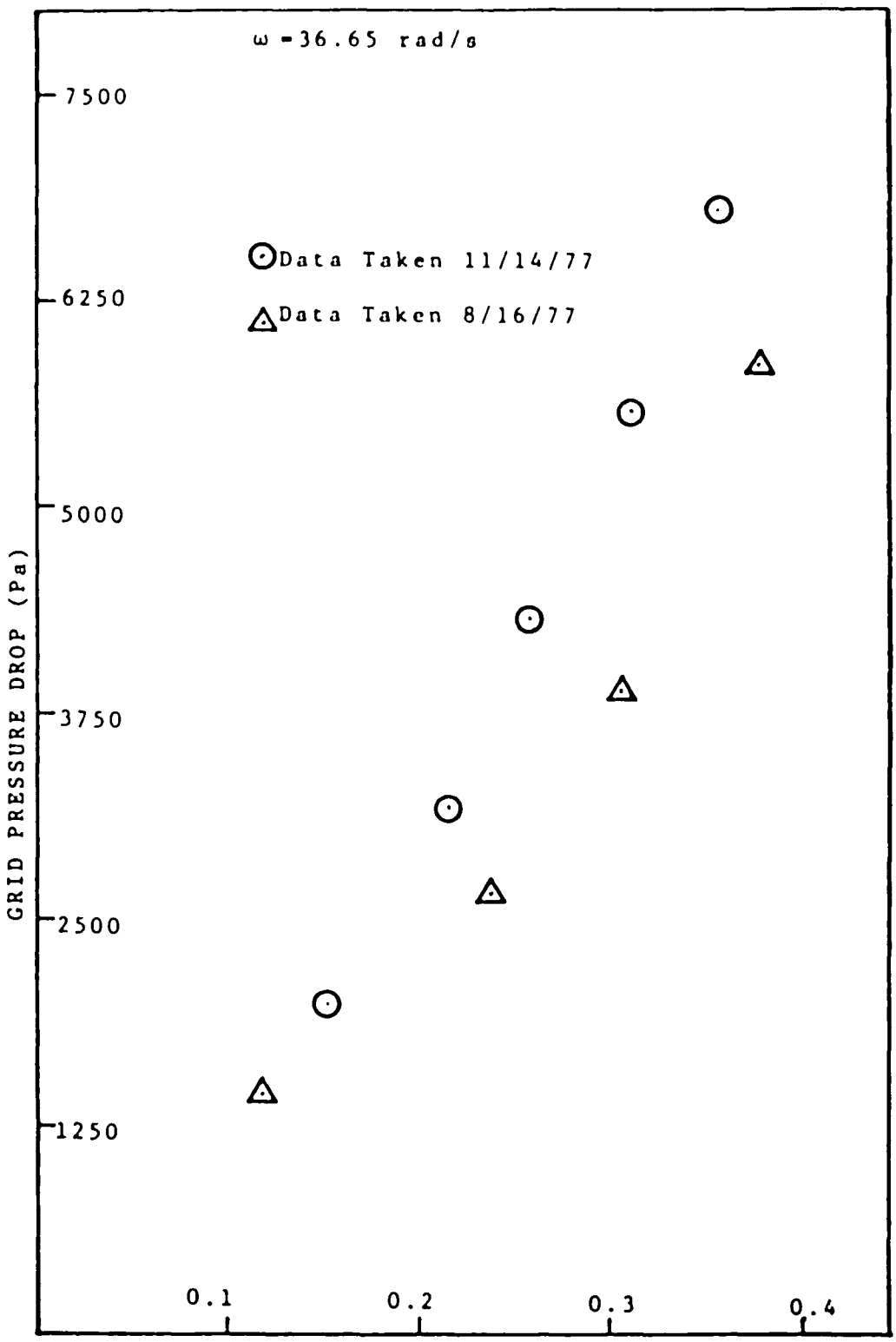

Fig. 19 Change in Grid Pressure Drop with Time

3. *Bed Pressure Drop*

In the experiments described in this chapter, the system was operated in a batch mode, where the bed material was added by pouring particles into the test section through the air exhaust hole at the top of the test section. In these tests the solids discharge tubes were closed and at the end of each test the bed material was removed manually from the test section.

In these experiments, the effect of angular velocity, air flow rate, particle size, and bed mass on minimum fluidization and bed pressure drop were determined.

The following procedures were used in performing the batch test: (i) The rotating plenum was vacuum cleaned completely, (ii) The discharge tubes remained closed, (iii) The desired amount of bed material was poured inside the plenum, (iv) The motor was started up and the angular velocity of the driving shaft was adjusted to match the desired strokoscope frequency, (v) To obtain a good distribution of particles over the entire height of the grid, the air flow rate was increased gradually until particle entrainment occurred. At this point the air flow rate was decreased gradually and the overall pressure drop was recorded at each flow rate. This procedure is called turndown, and the startup data were obtained with the bed initially at the bottom of the test section and pressure

drop was recorded as the air flow rate increased. Figure 20 shows that the difference between the two procedures is small. In most of the experiments, the turndown process was followed.

C. Discussion of Results

In Figures 20, 21, 22, 23, 24, and 26, the experimental data are compared with theoretical results from Martin's computer program. As was stated, the model for tangential velocity profile in the computer program is based on solid body rotation.

In all the experiments, the same particle size $\bar{d}_p$ = 410 x 10^{-6}m is used. Figures 20, 21, and 22 show the overall pressure drop, grid pressure drop and bed pressure drop for three different bed masses at ω = 36.65 rad/sec. These results are compared with each other in Figure 23 and as is shown, the minimum fluidization velocity is independent of the bed mass.

In Figure 24 the effect of angular velocity is shown on the bed pressure drop and fluidization conditions where the bed mass is constant.

Figure 25 shows the effect of particle size on bed pressure drop and minimum fluidization. These theoretical results are from Martin's computer program. As is shown, the particle size does not have any effect on the bed

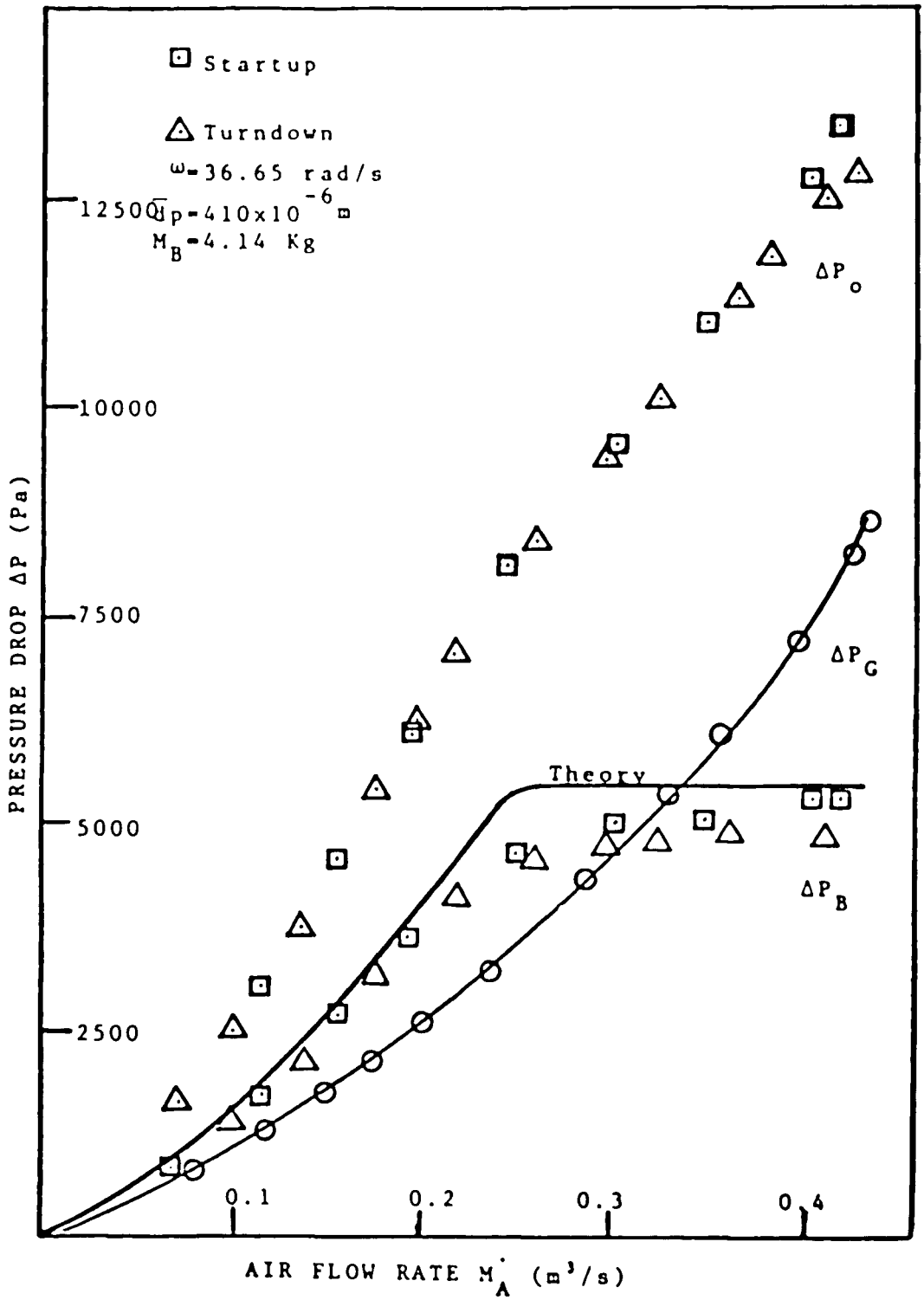

Fig. 20 Comparison Between Startup and Turndown

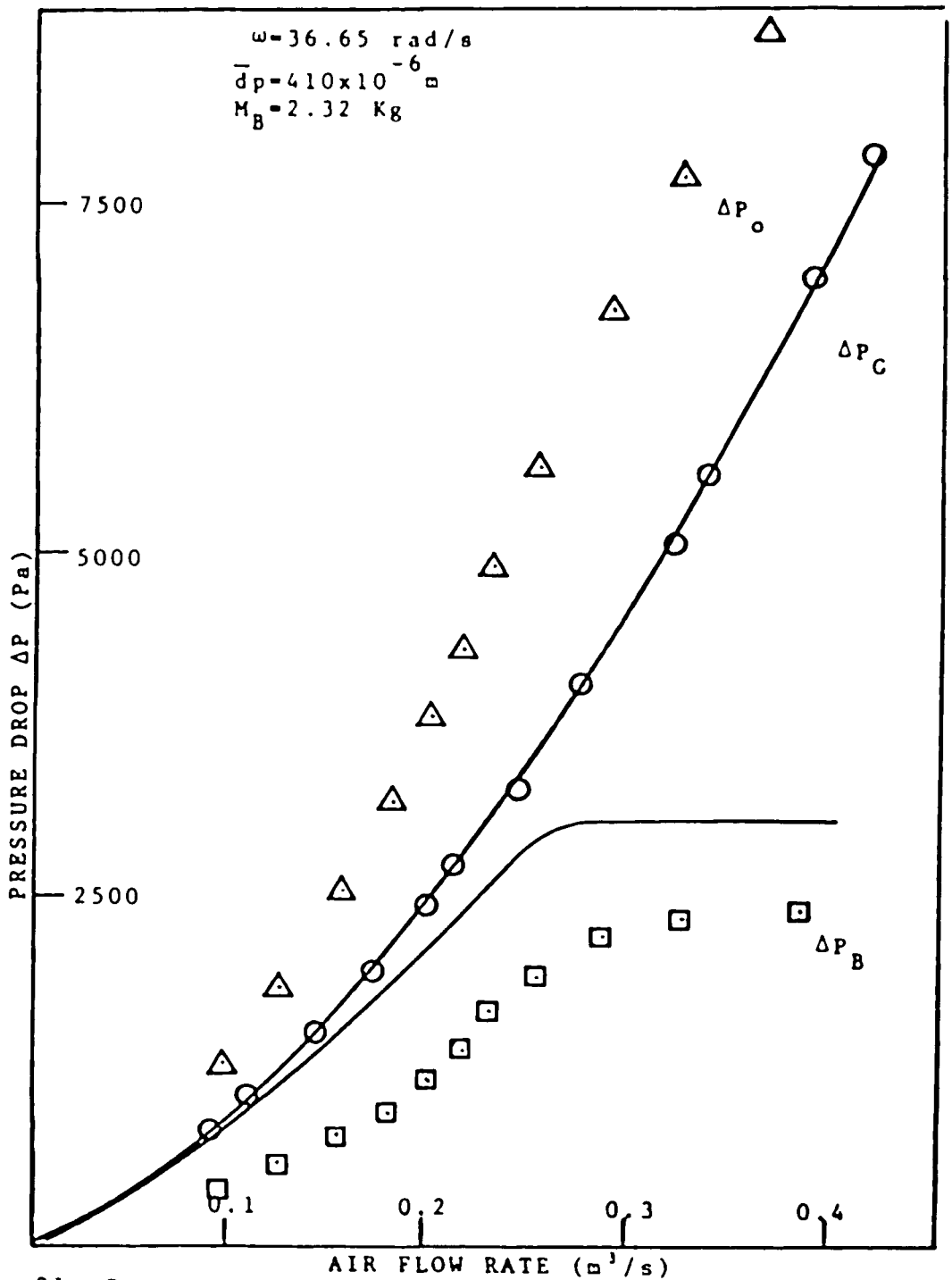

Fig. 21 Comparison Between Experimental Data and Theoretical Model for Bed Pressure Drop

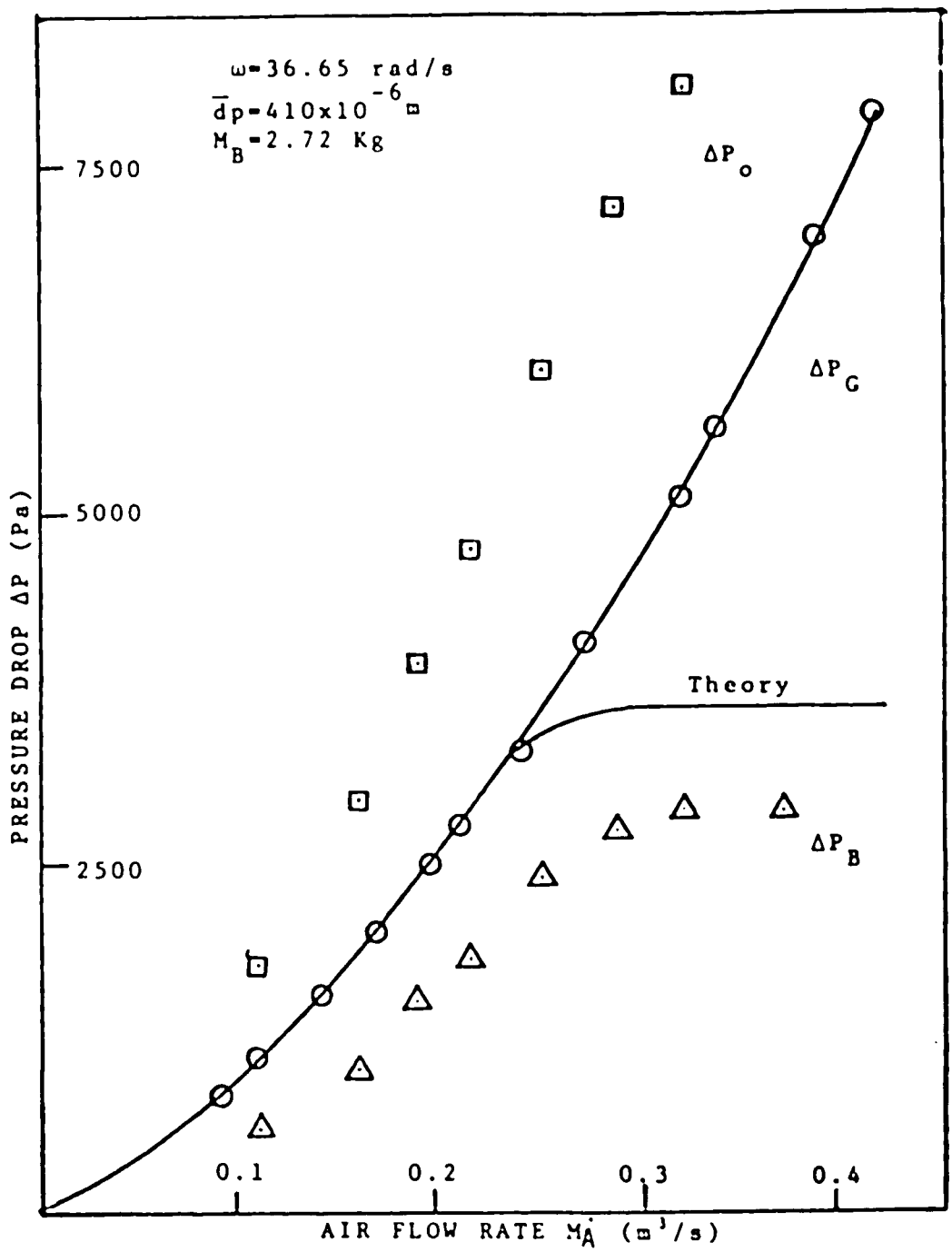

Fig. 22 Comparison Between Experimental Data and Theoretical Model for Bed Pressure Drop

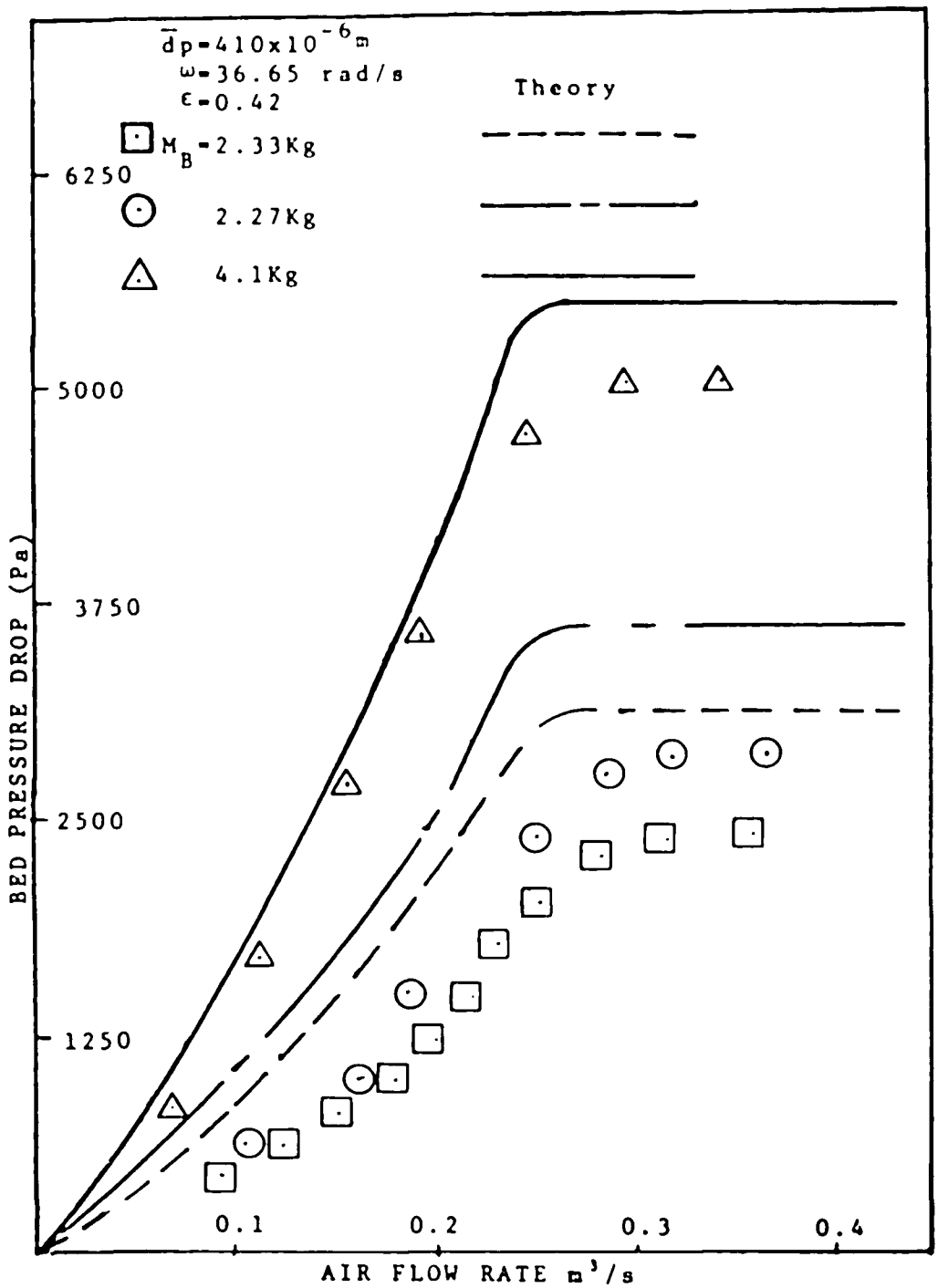

Fig. 23 Comparison Between Experimental Data and Theoretical Model for Pressure Drop for Different Bed Masses

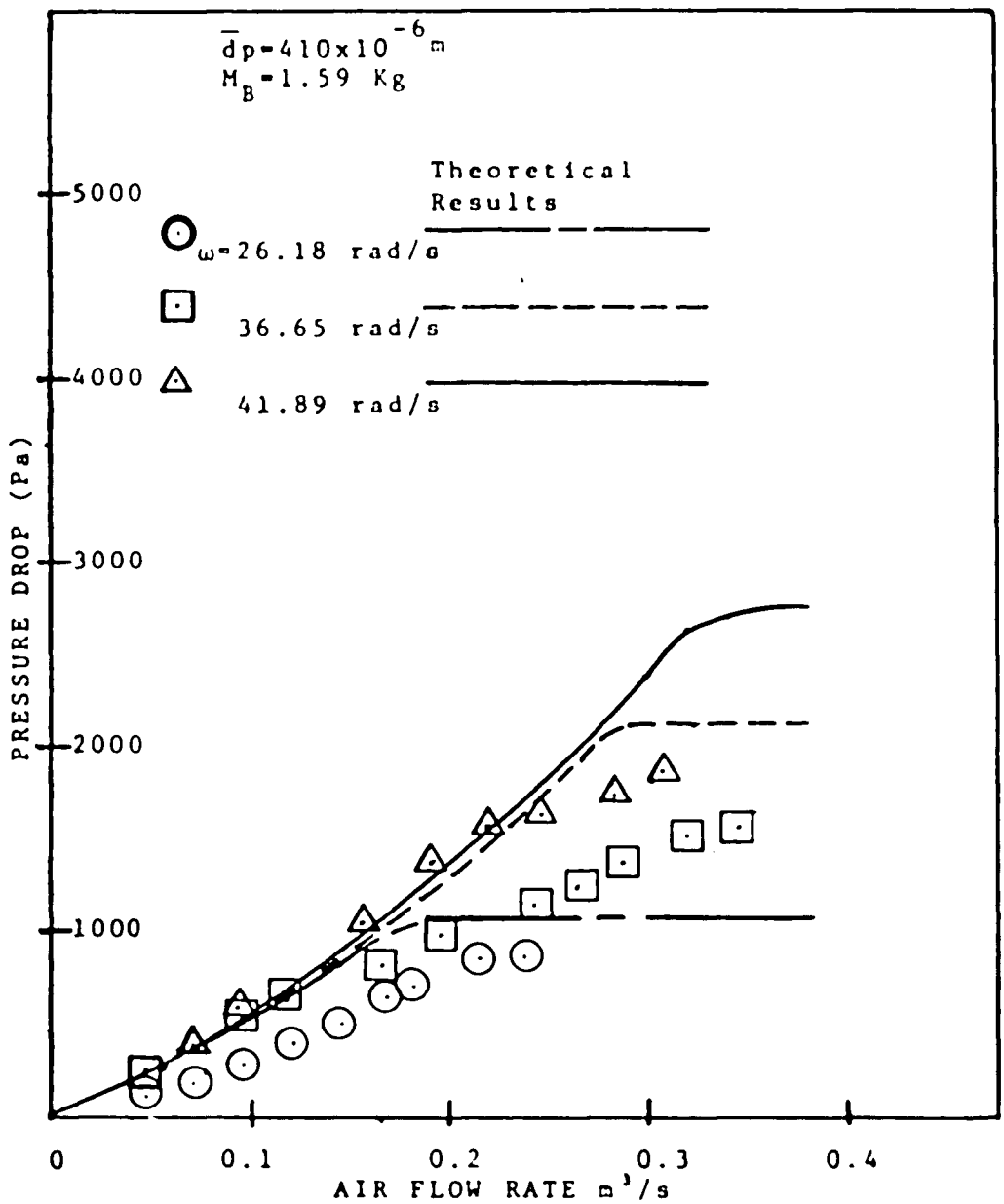

Fig. 24 Comparison Between Experimental Data and Theoretical Model for Pressure Drop for Different Angular Velocities

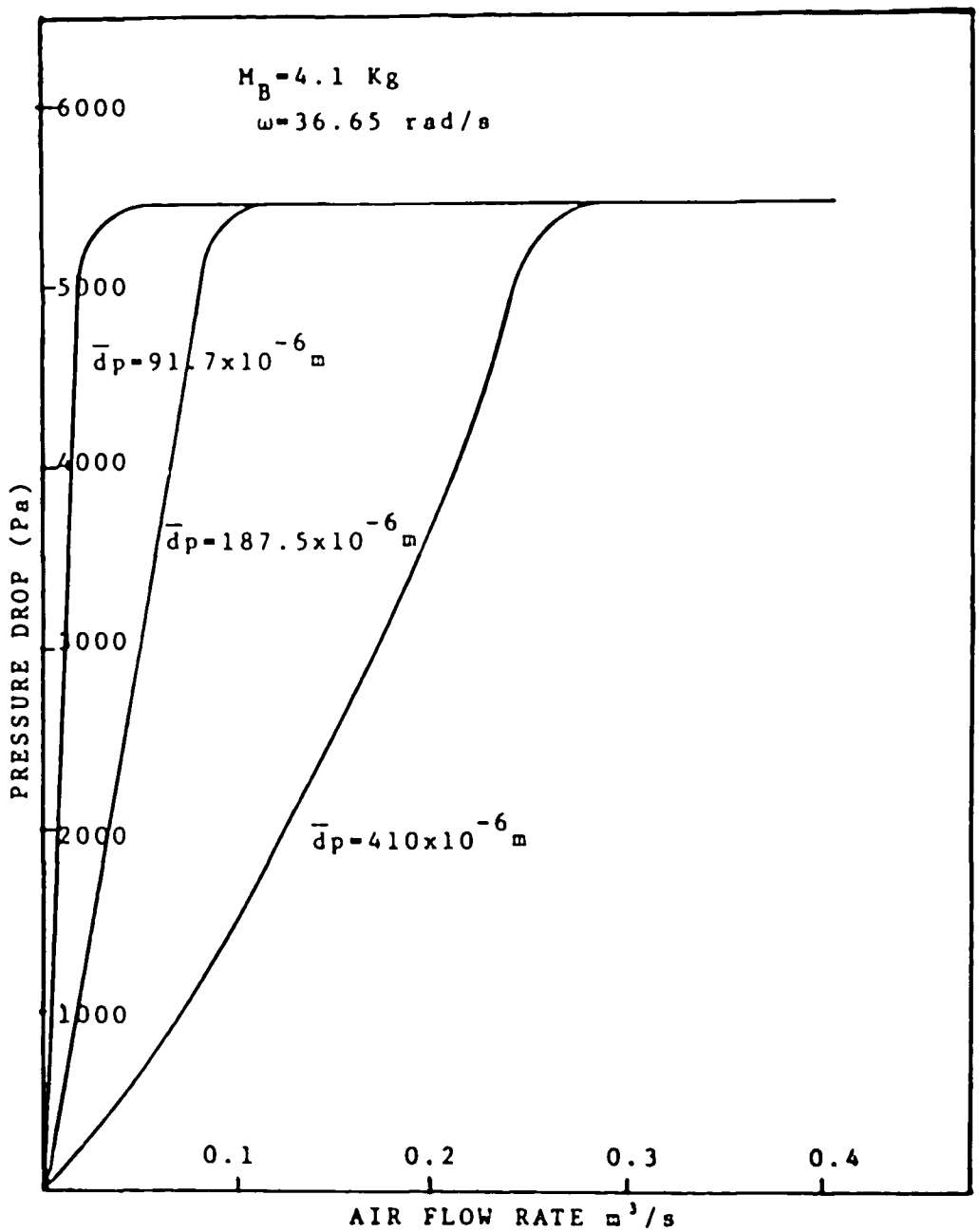

Fig. 25 Theoretical Results on Effect of Particle Size on Bed Pressure Drop

pressure drop at fluidization conditions, but it does affect pressure drop in the packed region. It also influences the point of minimum fluidization.

Figure 26 summarizes the batch experiments with a plot of bed pressure drop at minimum fluidization versus bed mass. The experimental data are compared with theoretical results for several different angular velocities. These results show that the theory overestimates bed pressure drop by 10 to 40 percent for the 410×10^{-6}m particles. As is seen in Figure 26, the discrepancy increases for higher angular velocities. Several things might be responsible for these discrepancies, including errors in the theoretical model, errors in measurement of pressure drop, angular velocity, bed mass, and particle elutriation. Particle elutriation was noted in several cases, and this could be responsible for the observed discrepancies.

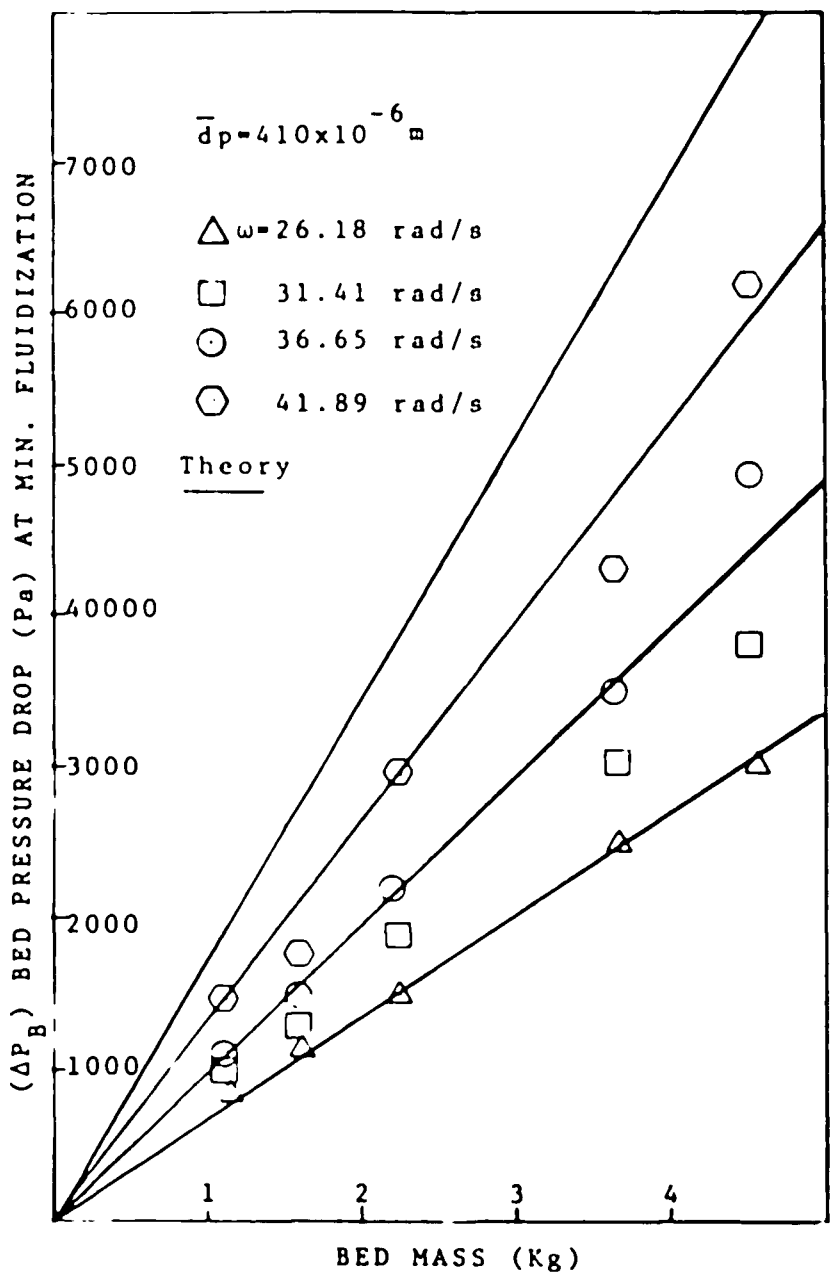

Fig. 26 Comparison Between Theory and Experiment for Pressure Drop at Minimum Fluidization Versus Bed Mass

IV. FEED AND REMOVAL OF SOLIDS

Experiments on the feed and removal of solids to the rotating bed are described in this section. Solids are fed through the feed tube, connected to the solids distributor plate at the base of the rotating chamber. Solids removal occurs through the six discharge tubes in the rotating grid. Load cells attached to the discharge bin permitted instantaneous measurement of solids discharge rate. In all of the tests the same particles with $dp = 410 \times 10^{-6}$ m and $\phi_s = 1$ were used.

In this chapter, the effects of (i) air flow rate (ii) angular velocity (iii) solids feed rate and (iv) geometry of discharge tubes are studied. The results of the overflow experiments are compared to those obtained in the batch experiments.

The following procedures were used in performing the overflow experiments: (i) The rotating plenum was vacuum cleaned completely, (ii) The load cells were connected to the power supply and digital volt meter, (iii) Pressure taps were connected to the 1.5 m manometer boards, (iv) The injection hose was connected to the feed tube, (v) The desired discharge tubes remained open, (vi) The motor was started up and the angular velocity of the bed was adjusted to match the desired

stroboscope frequency, (vii) The air supply valve was set on the desired air flow rate, (viii) The pressure drop across the grid at this air flow rate and angular velocity were recorded and (ix) The feed system was set on the desired condition and by opening the feed valve the test was started.

During experiments with continuous feed and removal, the system showed different behavior from that observed in the batch experiments. The particles were discharged from the test section when the thickness of the bed became greater than the depth of the discharge tubes in the chamber. All of the experiments described here were performed with the same length discharge tubes.

In this series of experiments, the bed mass is a function of the air flow rate. Therefore, in each test the air flow rate remained constant and the test was permitted to continue until the pressure drop remained constant. At the end of each test, the bed mass was weighed.

To determine whether the bed was packed or fluidized during a test, the results were compared with the results from the batch experiments. In addition, during the test, the state of the bed was checked regularly

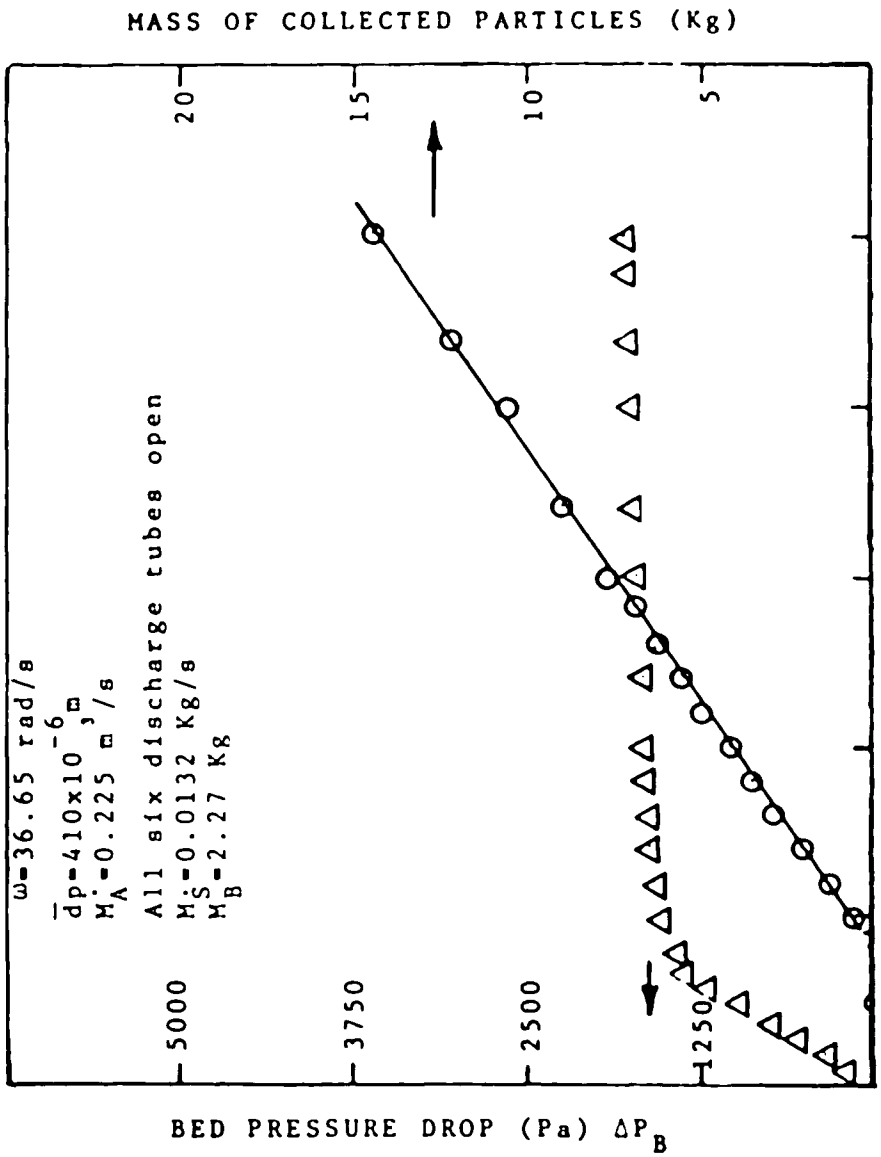

Bed Fig. 27 Bed Startup

through the air discharge opening at the top of the test section.

A. Dynamic Studies of Bed Startup

As was stated before, each test began with the test section empty and continued until steady state bed conditions were established. Figure 27 shows plots of bed pressure drop and mass of discharged bed material versus time. In this test, the air flow rate, angular velocity and particle feed rate were held constant and all six discharge tubes were open. As is shown, after four to five minutes the system reached a stable condition where the pressure drop remained constant and the mass of discharged material varied linearly with time. The rate of discharge given by the slope of the curve in Figure 27 is in good agreement with the measured solids feed rate. For the air flow rate and angular velocity used in this test, the bed was in packed condition.

1. Effect of Discharge Area

Figures 28 and 29 show the effect of discharge area on bed pressure drop and mass of discharged material. The two experiments in Figure 28 were performed with the same angular velocity, air flow rate and solids feed rate. By reducing the discharge area from six discharge

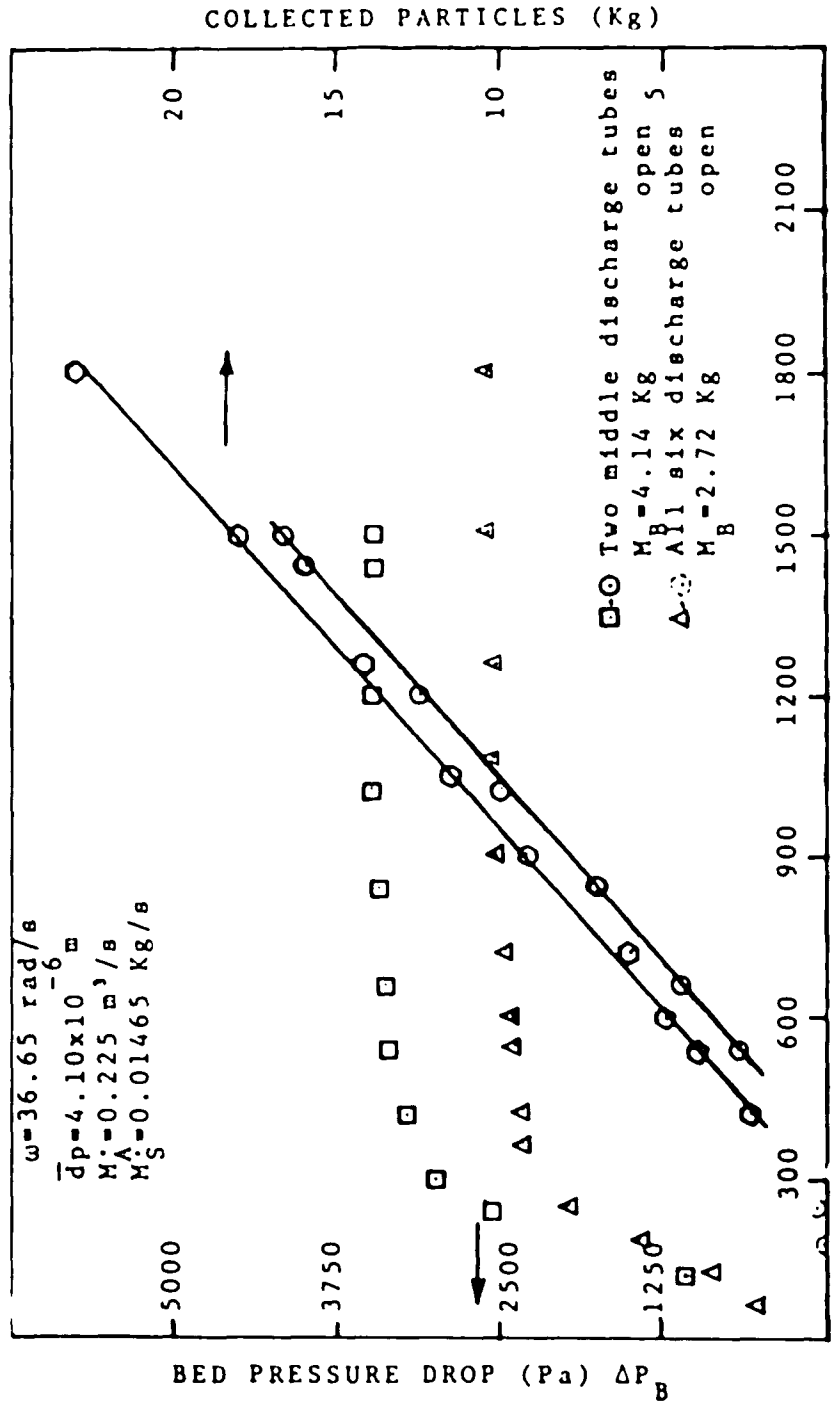

Fig. 28 Effect of Discharge Area on Bed Startup

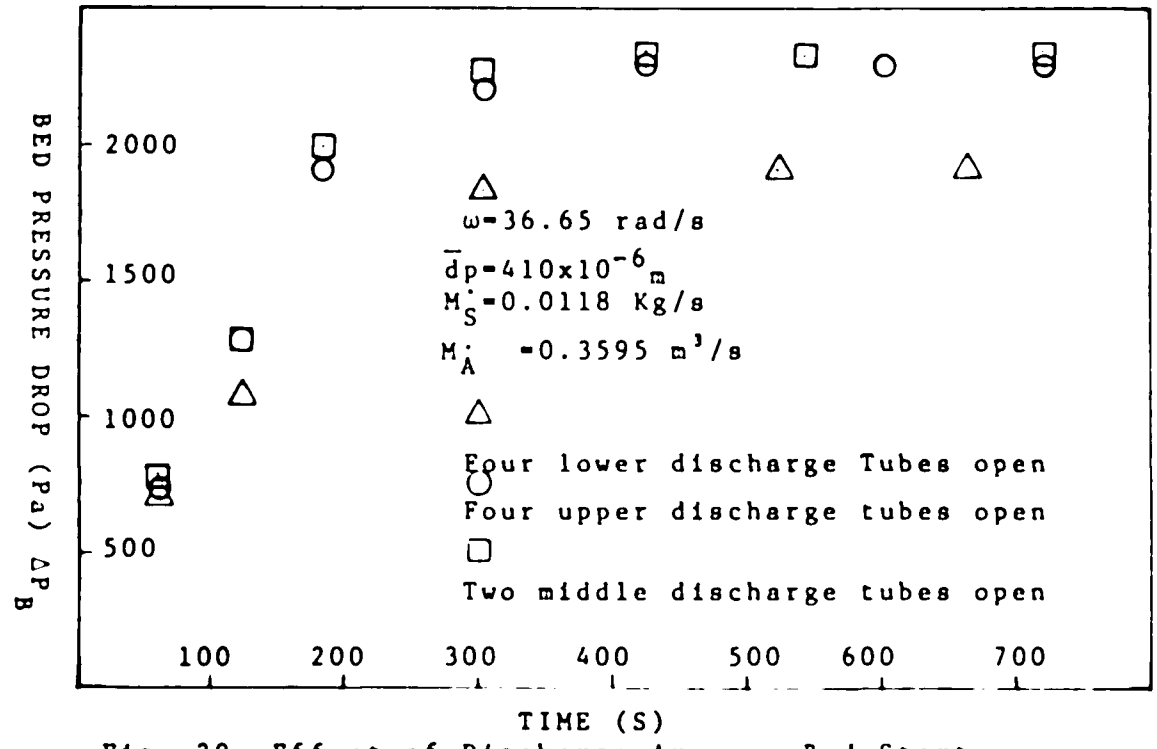

Fig. 29 Effect of Discharge Area on Bed Startup

tubes to two tubes (the middle two), the steady state bed pressure drop and bed mass both increased. The time required to achieve steady state conditions is slightly greater with the smaller discharge area, but once steady state is reached, the two discharge rates are equal to each other and to the reate of solids feed. In Figure 28, the air flow rate is below minimum fluidization and the bed is packed. Figure 29 shows the effect of discharge area at a higher air flow rate and lower solids feed rate. In this case the bed is fluidized and throughout the test the air flow rate, solids feed rate, and angular velocity were held constant.

These results suggest that the two upper discharge tubes have very little effect on discharge rate. More experiments are needed to determine the effects of the location of feed and removal points on system behaviors.

2. Effect of Particle Feed Rate

In Figures 30, 31, and 32 the effect of solids feed rate on bed pressure drop and discharge rate is studied. Figure 30 shows this effect on bed pressure drop for five different particle feed rates. With increasing feed rate, the steady state bed mass and bed pressure drop increase. In this figure, the bed was fluidized for all five experiments, the angular velocity and air

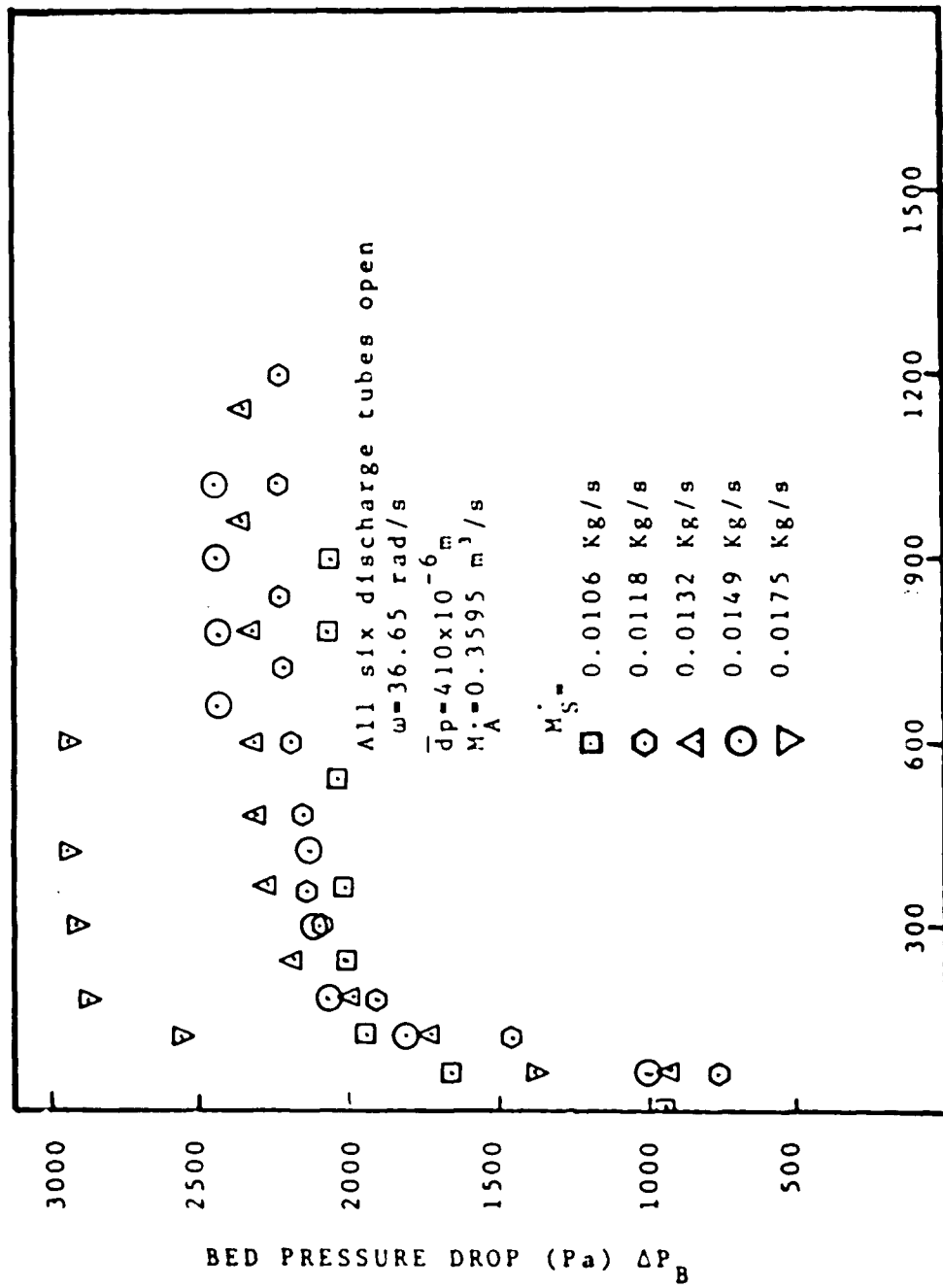

Fig. 30 Effect of Solids Feed Rate on Startup with Fluidized Bed

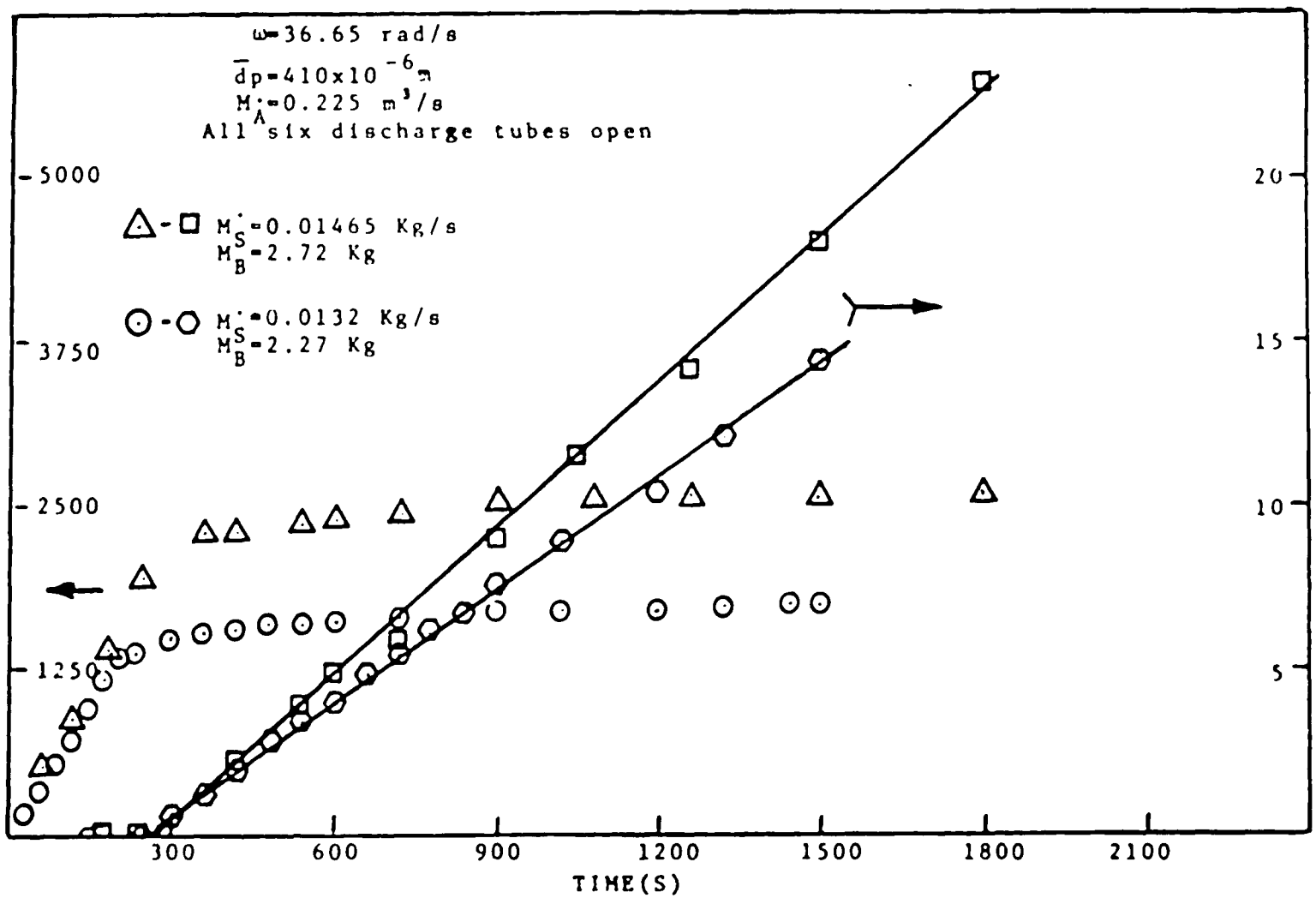

Fig. 31 Effect of Solids Feed Rate on Startup with Packed Bed

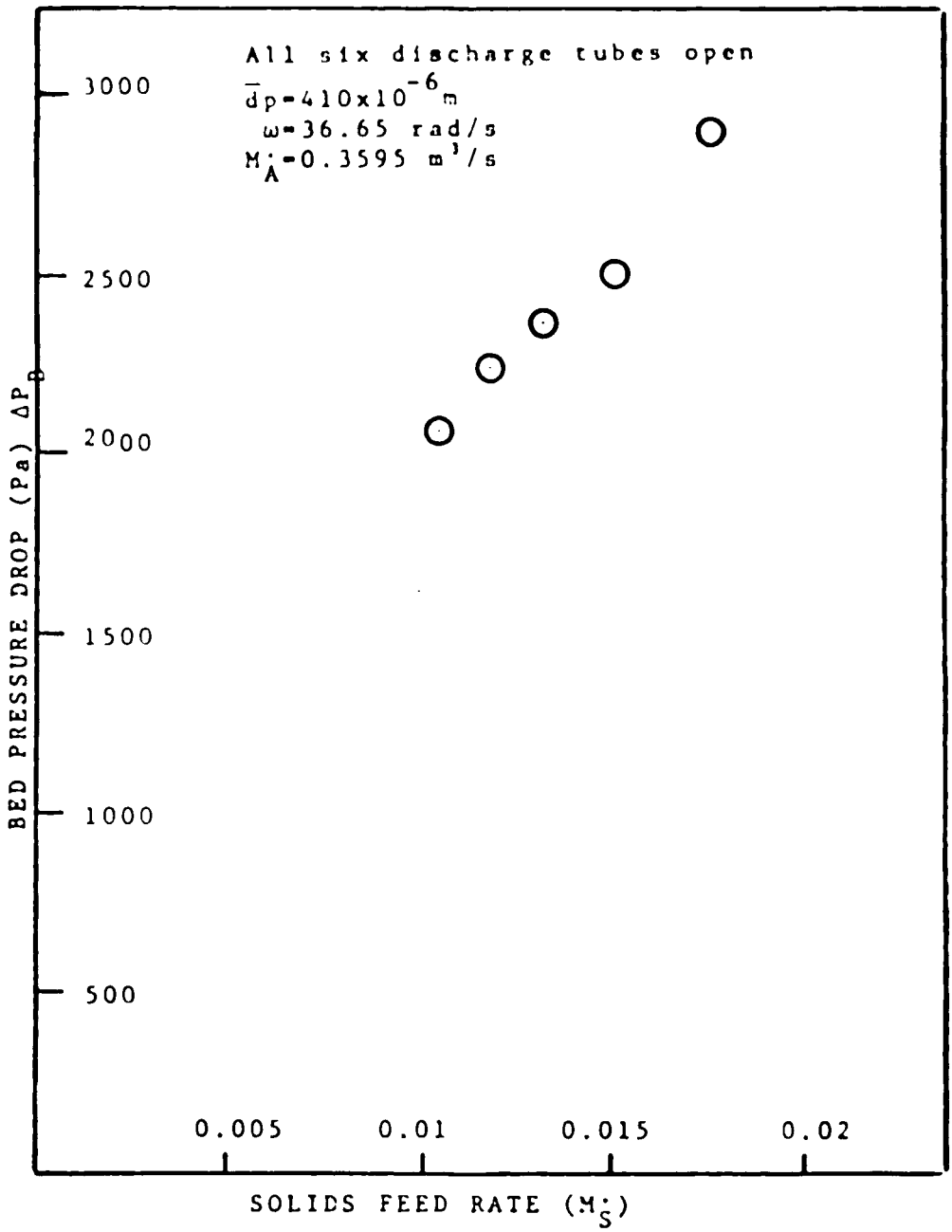

Fig. 32 Effect of Solids Feed Rate on Steady State Bed Pressure Drop

flow rate were held fixed and all six discharge tubes were open. Figure 31 shows similar results for a lower air flow rate (packed bed), where an increase in solids feed rate increases the solids discharge rate and the steady state bed pressure drop and bed mass. Figure 32 summarizes the influence of solids feed rate on steady state bed pressure drop for constant air flow rate, angular velocity and discharge area. For these conditions the bed was fluidized everywhere.

3. Effect of Angular Velocity

Figure 33, for constant solids feed rate, discharge area, and air flow rate, considers the effect of angular velocity on bed pressure drop. As is shown, the angular velocity has a great effect on steady state bed pressure drop and bed mass.

4. Effect of Air Flow Rate

Figure 34 considers the effect of air flow rate on the steady state bed pressure drop and discharge rate. As is shown by increasing the air flow rate, the bed mass and bed pressure drop are decreased, but once steady state is reached, the discharge rate doesn't change. In Figure 35, the effect of air flow rate on bed mass is studied. Each of these points belong to a separate test which has been performed with the same particle feed

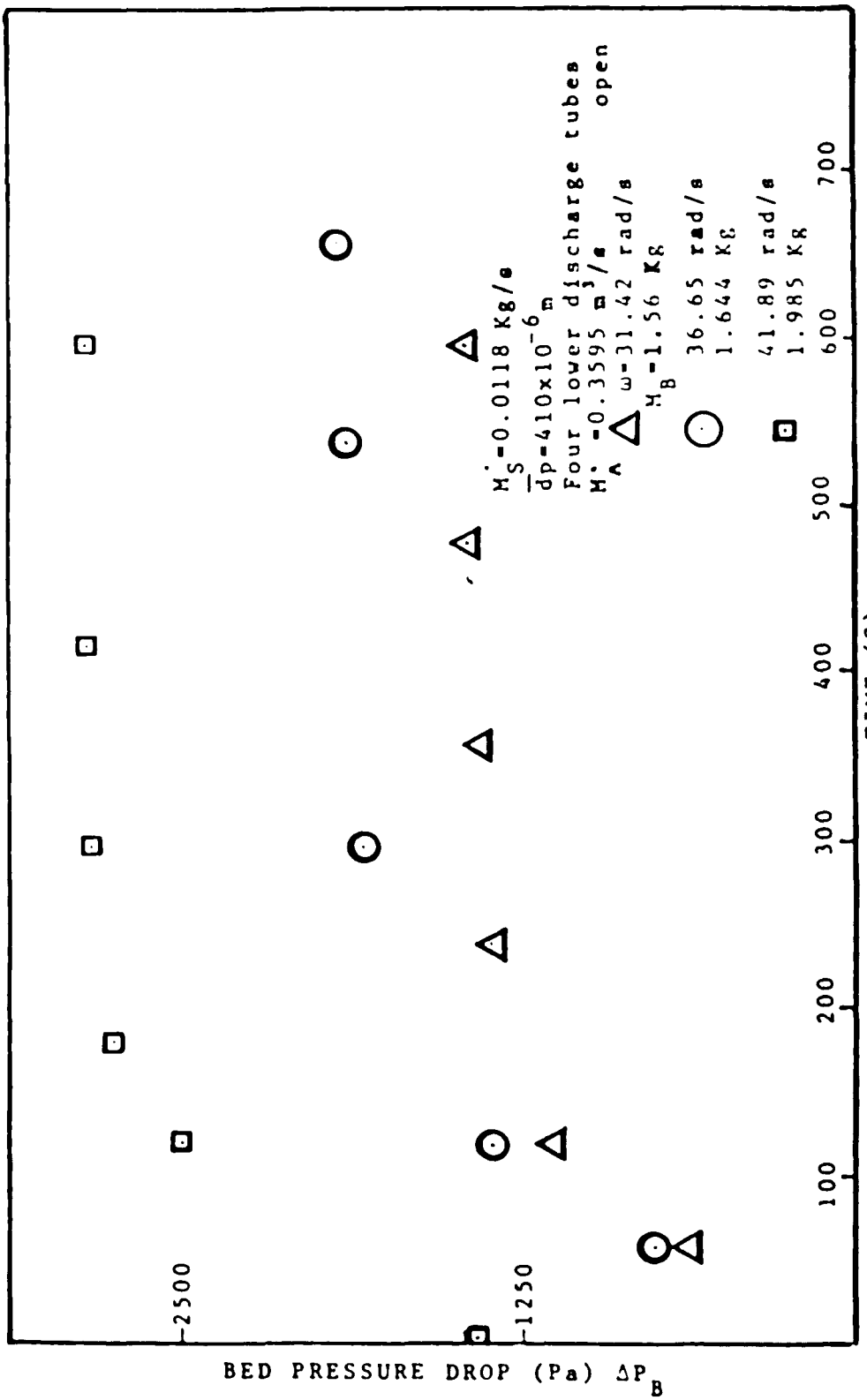

Fig. 33 Effect of Angular Velocity on Startup

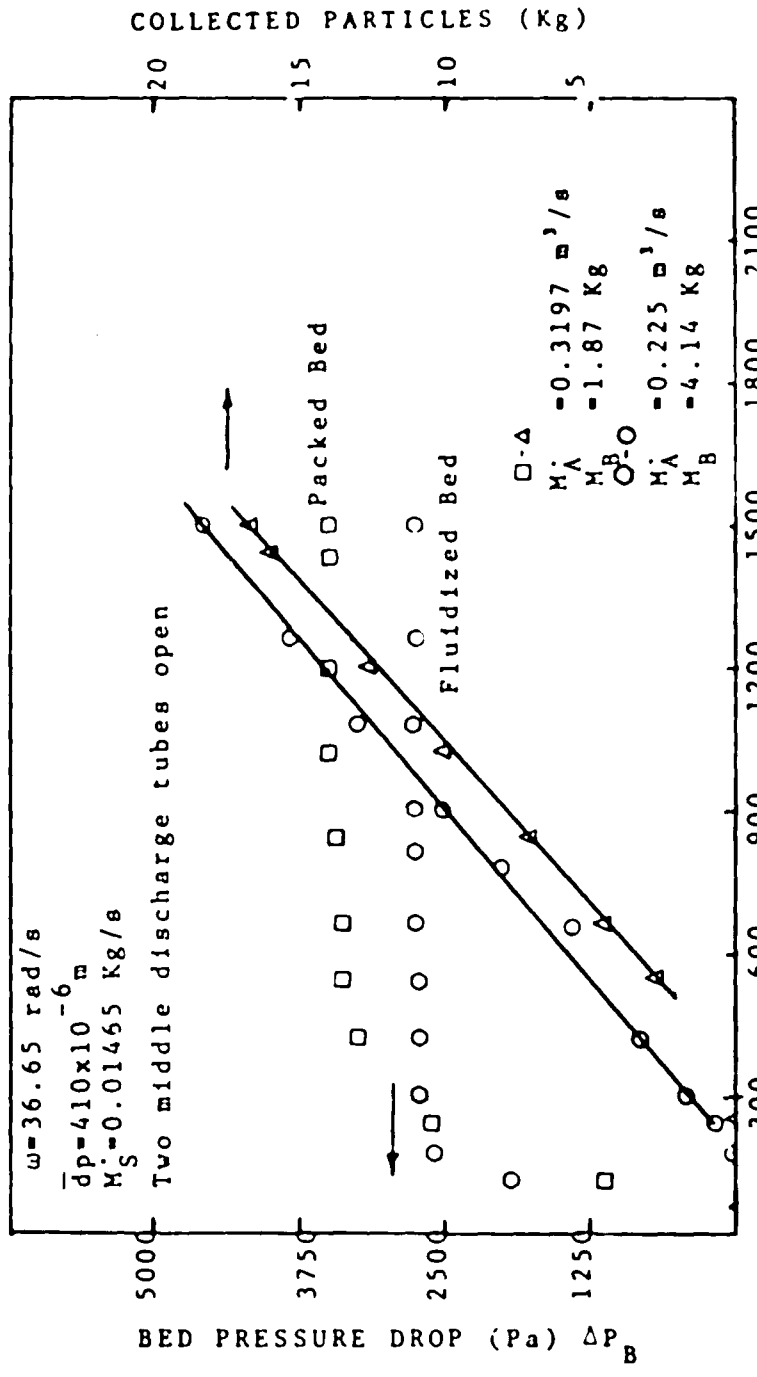

Fig. 34 Effect of Air Flow Rate on Startup

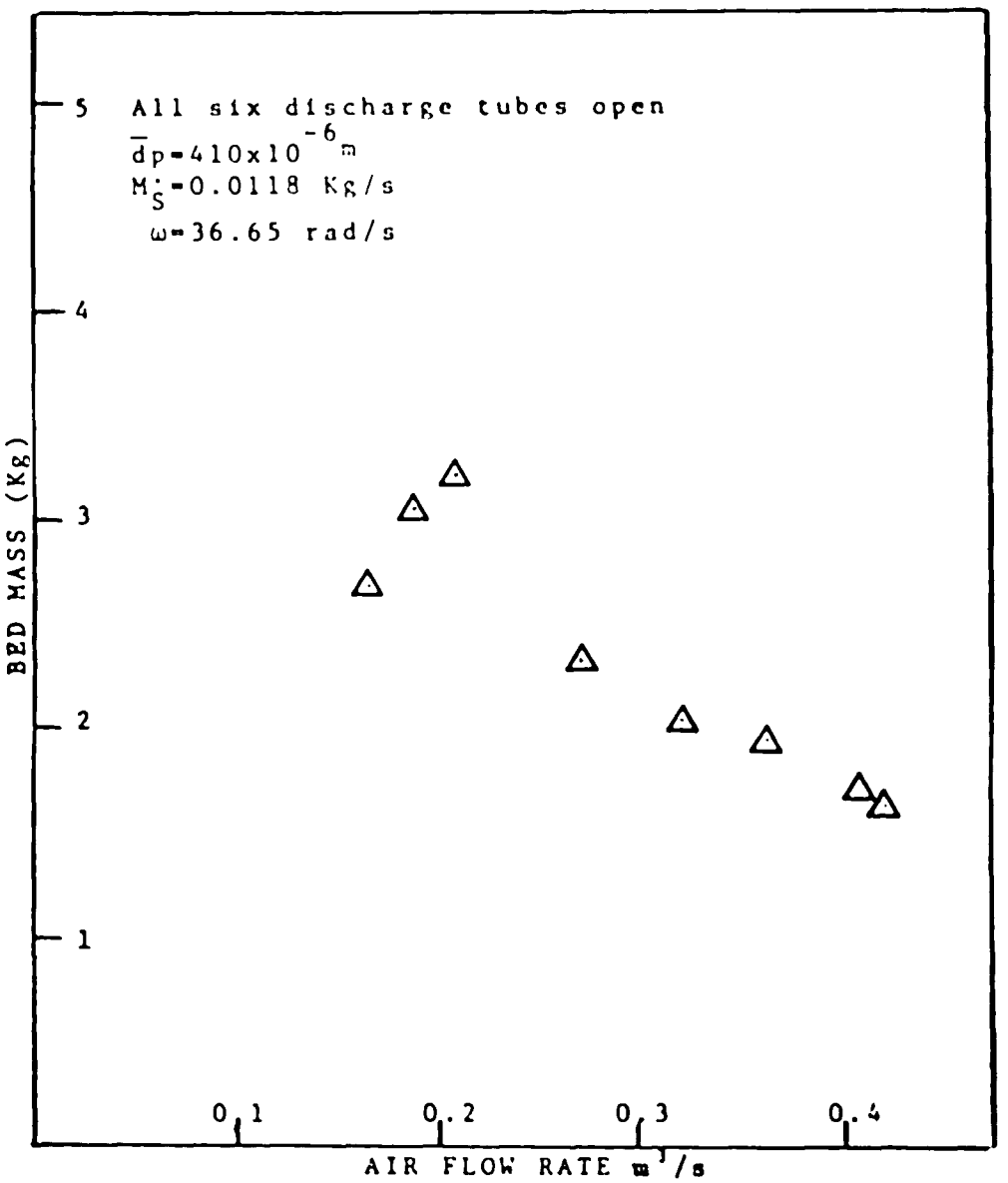

Fig. 35 Effect of Air Flow Rate on Steady State Bed Mass

rate, angular velocity, and discharge area but with different air flow rates. As is shown, there is a peak point corresponding to the reion of transition between packed and fluidized behavior.

Figure 36 shows the effect of air flow rate on bed pressure drop and the results are compared with the theoretical results for batch operation with a range of bed masses. In Figure 37, the same results are compared with the batch experiment results. Each of the overflow experiments points belong to a separate test with the same angular velocity, solids feed rate and discharge area. As is shown, the theory and experiments for batch operations are consistent with experiments for solids feed and removal. In the packed region, the bed mass increases slightly with air flow rate and the bed pressure drop depends on air flow rate according to the Ergun equation (equation for bed pressure drop at packed condition). In the fluidized region, the bed voidage increases with air flow rate, resulting in a decrease in bed mass and bed pressure drop with air flow rate. When fluidized, the actual steady state masses measured in the overflow experiments give values for bed pressure drop which are in reasonable agreement with the theoretical and experimental values for batch operation.

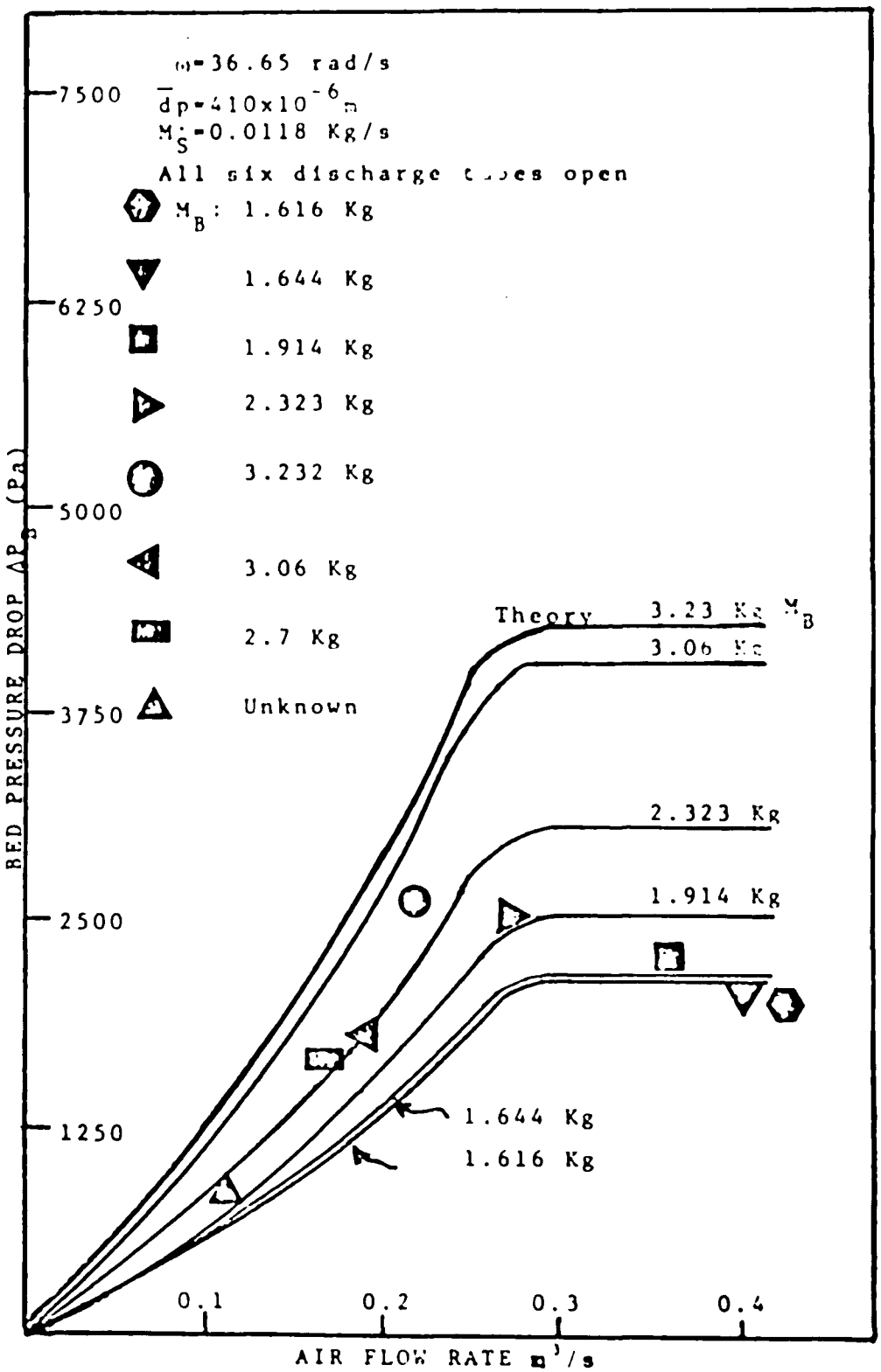

Fig. 36 Comparison Between Batch Theory and Data from Overflow Experiments

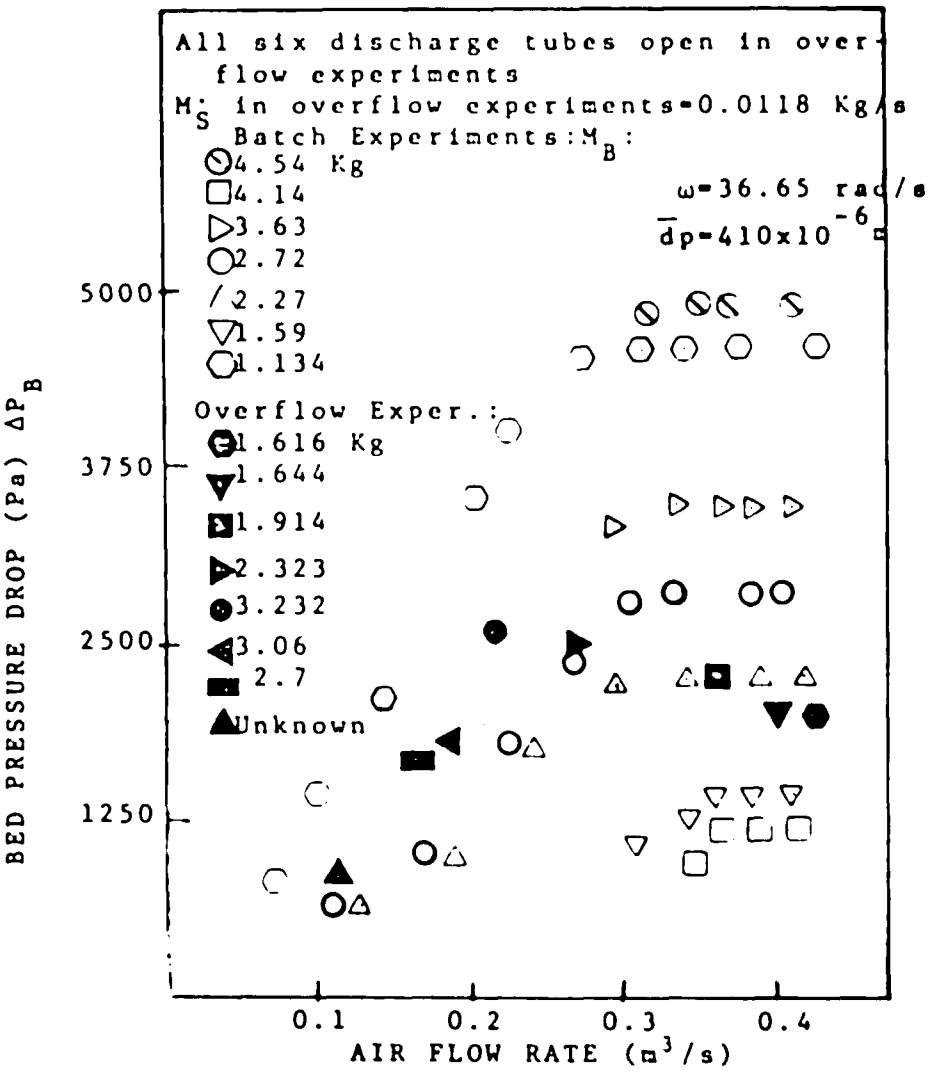

Fig. 37 Comparison Between Data from Batch and Overflow Experiments

As was observed, it usually takes close to five minutes in all cases until the system reaches steady conditions. Many more experiments should be performed and the results presented here should be thought of as a preliminary study of the behavior of a rotating fluidized bed with continuous feed and removal.

V. CONCLUSIONS AND RECOMMENDATIONS

This study of bed pressure drop and minimum fluidization in the centrifugal fluidized bed (CFB) shows that in the batch experiments, the theory over estimated bed pressure drop by 10 to 40 percent. The experimental results from the overflow experiments are consistent with the batch results. During the tests, elutriation of particles was observed both in the batch and overflow experiments. In all of the batch experiments, the bed masses were measured before starting each test; but in overflow, this procedure was done after each test. For this reason the discrepancy between the results could be caused by this parameter. However, more experiments need to be done on the effect of elutriation.

Studies of the effect of air flow rate on the overflow experiments show different behavior from that observed in the batch experiments. This is due to the effect of air flow rate on bed voidage and bed mass.

As a whole, the model for fluidized bed pressure drop, which assumes solid body rotation of the bed, gives good agreement with experimental results for the batch and overflow experiments.

The following recommendations for future investigations are suggested: (i) more experiments need to be

done on batch experiments with this apparatus, (ii) studies of elutriation during batch and overflow operation should be performed. The use of a cyclone at the top of the test section is recommended, (iii) more experiments on the characteristics of the feed and removal systems should be done, (iv) in all experiments within this thesis just one particle size ($\overline{dp} = 410 \times 10^{-6}$m) was used. Experiments should be performed with other particle sizes, (v) more experiments need to be done to determine the effect of angular velocity on system behavior in overflow operation, (vi) bubble behavior needs to be studied in the overflow experiments, (vii) a photographic study of overflow experiments is suggested, (viii) the test section should be modified to study the effect of heat transfer in a CFB, and (ix) it would also be interesting to operate the apparatus at a different angle relative to the vertical position.

REFERENCES

1. Hotel, H.C. and Howard, J.B., New Energy Technology - Some Facts and Assessments, Cambridge, Mass., The MIT Press, 1971.

2. Katy, D.L. and Williams, B., "Fluidized Bed Combustion", Evaluation of Coal Conversion Processes to Provide Clean Fuels, Part II, NTIS, 1974, pp. 6-13.

3. Brown, G.E., Farkas, D.F., "Centrifugal Fluidized Bed", Food Technology, Dec. 1972, pp. 23-30.

4. Levy, E.K., Dodge, C., Chen, J., "Parametric Analysis of a Centrifugal Fluidized Bed Coal Combustor", ASME Publication 76HT - 68, 1976.

5. Martin, N.W., "Mechanics of Fluidization in Centrifugal Beds, M.S. Thesis, Lehigh University, 1977.

6. Metcalfe, C.I. and Howard, J.R., "Fluidization and Gas Combustion in a Rotating Fluidized Bed'. Applied Energy (3), 1977, pp. 65-74.

7. Levy, E.K., Martin, N., Chen, J., "Minimum Fluidization and Startup of a Centrifugal Fluidized Bed", Cambridge University Press, England, 1977.

8. Kunii, D. and Levenspiel, O., Fluidization Engineering, New York, New York, John Wiley and Sons, Inc., 1969.

APPENDIX - A

RADIAL VARIATION OF TANGENTIAL VELOCITY

Three concentric regions with different kinds of tangential velocity profiles are defined for a centrifugal fluidized bed (CFB). As shown in Figure A-1, these are the viscous core region (A), the potential vortex region (B) and the bed region (C).

Information on the radial variation of tangential velocity is needed in computing the bed pressure drop.

Two possible velocity profiles are postulated in reference 7. These are: (1) solid body rotation and (2) uniform tangential velocity.

Recent experiments show that the data from pressure drop measurements are in better agreement with the solid body assumption than the uniform tangential velocity [5]. Experiments also show that axial and radial flows seem to stagnate for radii close the axis of rotation. An acceptable model for tangential velocity in the core (region A) [6] is:

$$V_\theta = \left(\frac{r_1}{r_c}\right)^s \omega r$$

In region B, a potential vortex is assumed and after considering angular momentum for inviscid flow, the boundary conditions yield:

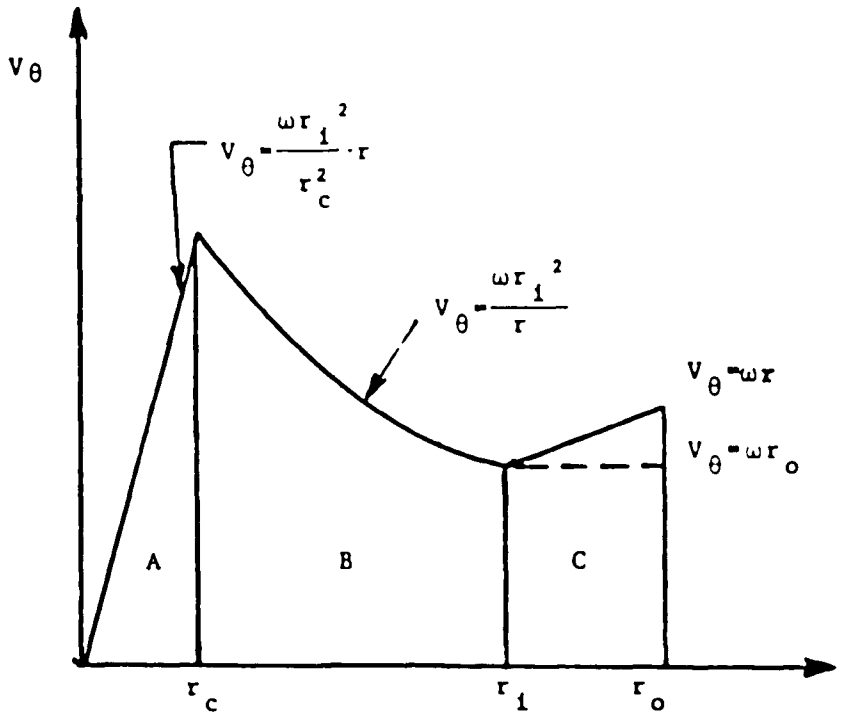

Fig. (A-1) Postulated Tangential Velocity Profiles

$$V_\theta = r_i^2 \frac{\omega}{r}$$

For the third region as was stated before, two models were suggested. For solid body rotation:

$$V_\theta = \omega r$$

and for uniform tangential velocity:

$$V_\theta = \omega r_o$$

APPENDIX - A

SHAPE OF THE BED (from Reference 5)

Assuming the CFB behaves like a liquid, the bed surface can be assumed to be perpendicular to the resultant of the local acceleration vectors as shown in Figure B-1:

$$\tan\theta = \frac{g}{\omega^2 r_i} = \frac{dr_i}{dx} \quad , \quad r_i^2 = \frac{2gx}{\omega^2} \tag{1}$$

where $X = X_1 + Z$.

The volume of bulk solids in the bed is equal to:

$$\frac{m}{\rho_s(1-\varepsilon)} = \int_{X=X_1}^{X=X_1+H} \pi(r_o^2 - r_i^2)dx \tag{2}$$

The outer radius (r_o) is a function of grid taper angle and is calculated from the following equation:

$$r_o = X\tan\alpha + r_{o2} - (X + H)\tan\alpha \tag{3}$$

By solving equations 1, 2, and 3 we will have:

$$X_1 = \frac{\omega^2}{2gH}\left(\frac{H^3}{3}\tan\alpha^2 - H^2 r_{o2}\tan\alpha + Hr_{o2}^2 - \frac{m}{\pi\rho_s(1-\varepsilon)} - \frac{gH^2}{\omega^2}\right)$$

$$r_i = \frac{\sqrt{2g(X_1+Z)}}{\omega}$$

$$r_o = (X_1+Z)\tan\alpha + r_{o2} - (X_1+H)\tan\alpha$$

In the above equation, Z is the height above the chamber floor. Integration of equation (2) requires that the bed completely covers the grid. Now if for any reason it doesn't, and instead just climbs to some unknown height, h', as shown in Figure (B-2), we have:

$$\int_{Z=0}^{Z+h'} \pi(r_o^2 - r_i^2)dZ = \frac{m}{\rho_s(1-\epsilon)} = \text{volume of the bed} \qquad (4)$$

$$r_o = Z\tan\alpha + r_{o1}$$

$$r_i = \frac{\sqrt{2g(Z+X_1)}}{\omega}$$

From boundary conditions, at $Z = h'$, $r_o = r_i$, we have:

$$\frac{2g(Z+X_1)}{\omega^2} = h'^2\tan^2\alpha + 2r_{o1}h'\tan\alpha + r_{o1}^2 \qquad (5)$$

Now if we solve for X_1 in term of h':

$$X_1 = \frac{\omega^2}{2g}(h'^2\tan^2\alpha + 2r_{o1}h'\tan\alpha + r_{o1}^2 - \frac{2gh'}{\omega^2}) \qquad (6)$$

by solving integral equation 4, using digital computer techniques:

$$\frac{h'^2}{3}\tan^2\alpha + r_{o1}h'^2\tan\alpha + r_{o1}^2h' - \frac{gh'}{\omega^2}(h'-2gX_1) =$$

$$\frac{m}{\pi\rho_s(1-\epsilon)} \qquad (7)$$

by using equations 6 and 7, h', X_1 will be found.

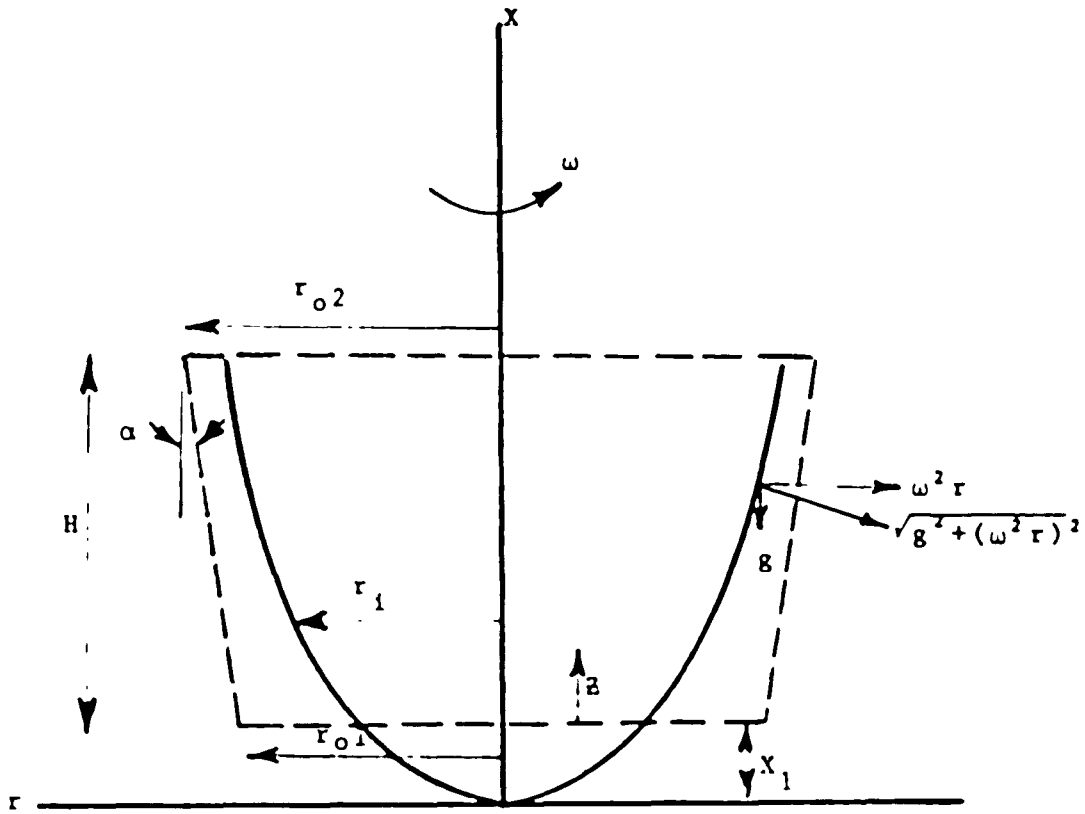

Fig. (B-1) Coordinate System for Analysis of Bed Shape Where Bed Covers Grid

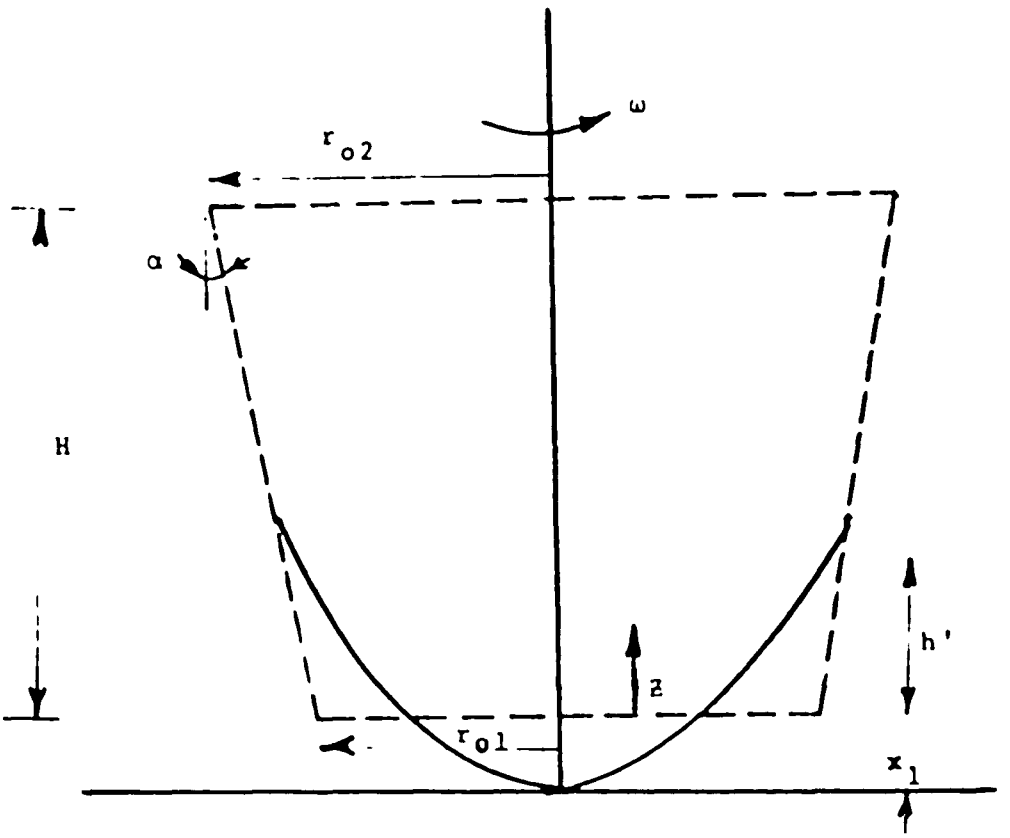

Fig. (B-2) Coordinate System for Analysis of Bed Shape Where a Portion of Grid is Exposed

APPENDIX - C

CALCULATION OF BED PRESSURE DROP BY COMPUTER ANALYSIS

(from Reference 5)

When the bed thickness is nonuniform, with the aid of the digital computer, a solution for bed pressure drop as a function of gas flow rate can be determined. This program takes into consideration the axial variation of bed thickness, itself a function of angular velocity, bed mass, and grid geometry.

The fluidizing gas is subject to an overall pressure drop, ΔP_o, as it flows from the plenum to the freeboard. The quantity ΔP_o consists of three terms:

1 - Grid pressure drop (ΔP_G)

2 - Bed pressure drop (ΔP_B)

3 - Freeboard pressure drop

In all of our experiments, we consider grid pressure drop and freeboard pressure drop together and therefore

$$\Delta P_o = \Delta P_G + \Delta P_B$$

At any height Z, the inside radius of the bed r_i may be calculated [Figure (C-1)] using the liquid model for bed shape. The grid pressure drop (ΔP_G) is approximately a parabolic function of gas velocity,

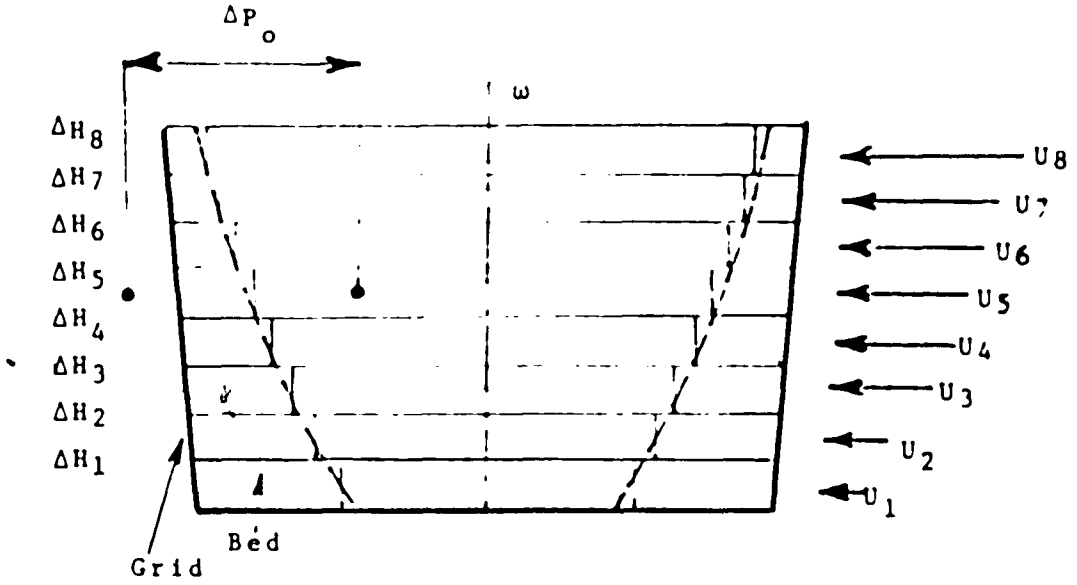

Fig. (C-1) Model of Bed Pressure Drop for Numerical Analysis

U_o, so that

$$P_G = K_1 U_o^2 + K_2 U_o$$

where K_1 and K_2 can be determined experimentally for each of the grids used, thus $\Delta P_G(U_o) = \Delta P_G$.

If the bed is packed, the Ergun equation for packed pressure drop reveals that $\Delta P_{BP} = \Delta P_{BP}(U_o, r_o, r_i)$. If the bed is fluidized, in this case gas velocity is higher than the minimum fluidizing velocity which was described before. In this case, $\Delta P_{BF} = \Delta P_{BF}(r_o, r_i)$. Mathematical expressions have been determined for all of these cases and a digital computer solution for bed pressure drop as a function of gas flow rate has been derived [5].

In this computer program, first ΔP_o is assigned a very low arbitrary value. For this small overall pressure drop, the computer solves for the velocity through the first bed "ring" of incremental height, H, by using the relations

$$\Delta P_o = \Delta P_G + \Delta P_{BP}$$

The minimum fluidizing velocity is calculated for the incremental ring under consideration. If the velocity computed is greater than the minimum fluidizing velocity, then

$$\Delta P_o = \Delta P_G + \Delta P_{BF}$$

and the velocity through the ring must be recalculated using the fluidized relation for ΔP_o. In any case, the correct value for local superficial velocity is found, and the mass flow rate through the first ring of incremental height is determined.

$$[m^o = \rho_f U_o \cdot dA]_{\cdot} = [\rho_f U_o 2\pi r_o \Delta H_1]_1$$

Similar computations are made for the second ring of height H_2, and the third, and so on. The mass flow rates through each are summed until the flow through the entire peripheral area of the bed is determined. Causing the axial variation of radial mass flow rate per grid height, the computer is made to loop back repeatedly to the arbitrary overall pressure drop, increasing it incrementally with each loop. A new gas flow rate and pressure drop are determined each time, and by these results it is possible to determine pressure drop versus gas flow rate.

APPENDIX - D

EFFECT OF GRID RESISTANCE ON FLUIDIZATION (from (Reference [5])

The experiments indicate that startup of the fluidized bed system is strongly dependent on grid characteristics and may be impossible without a well designed grid.

During startup, the gas should pass through the resistances caused by the grid and the bed. Suppose the grid resistance is much smaller than the bed resistance. In this case, when the bed is in the slumped condition, as occurs during startup, a portion of the grid is not covered by the bed, so because the grid resistance is much smaller than the bed resistance, velocities at the boundary of the bed and uncovered grid are very high compared with velocities through the bed. For such a low grid pressure drop, the bed may simultaneously exhibit different regions demonstrating elutriation, fluidization, and packed characteristics, depending on local bed thickness (Figure D-1a). Now if the grid resistance is much larger than the bed resistance, in this case, the flow through the grid is not a strong function of Z, since the bed thickness has a relatively small effect on axial variations of radial flow. Thus, the flow is nearly uniform (Figure D-1b),

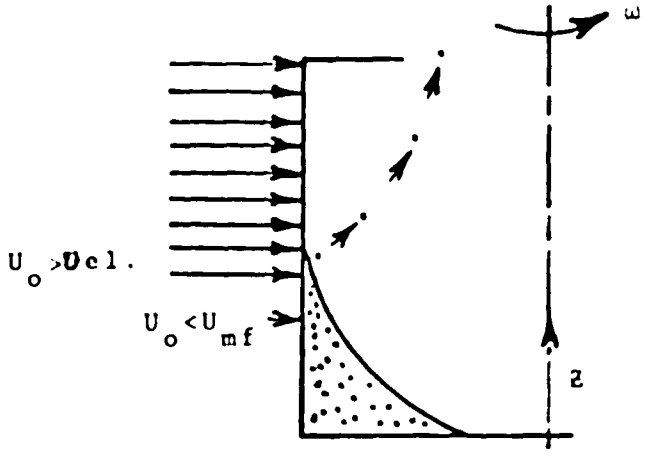

(a)
Grid Resistance<<Bed Resistance

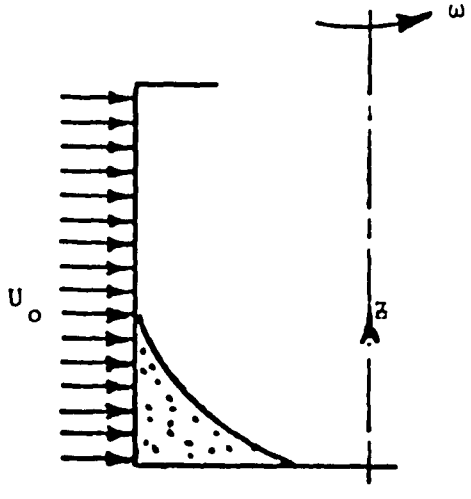

(b)
Grid Resistance>>Bed Resistance

Fig. (D-1) Effect of Grid Resistance on Flow Uniformity

and uniform fluidization is possible through the bed which might be nonuniform in thickness and not fully distributed over the grid. Therefore, startup is always possible if a high enough grid resistance is used. More uniform bed thicknesses require larger grid resistances in order to achieve complete fluidization before elutriation.

It is of great practical importance that the bed be as uniform as possible, at least covering the entire grid, so that the grid resistance can be low and still allow startup of the system.

A series of experiments were conducted to determine a grid geometry which would allow the bed to distribute itself more evenly over the grid. Initially, studies deduced that a truncated conical grid with a taper angle of 22° would solve the problem of startup, allowing the particles to distribute themselves over the grid periphery. The idea worked perfectly as long as the bed was operated in packed regime. However, once the bed reached minimum fluidizing conditions, it began to behave like a liquid, shifting to the top of the grid (Figure D-2b), and the problem of bed nonuniformity resulted once again. It was deduced that, due to the liquid-like character of the fluidized particles, a

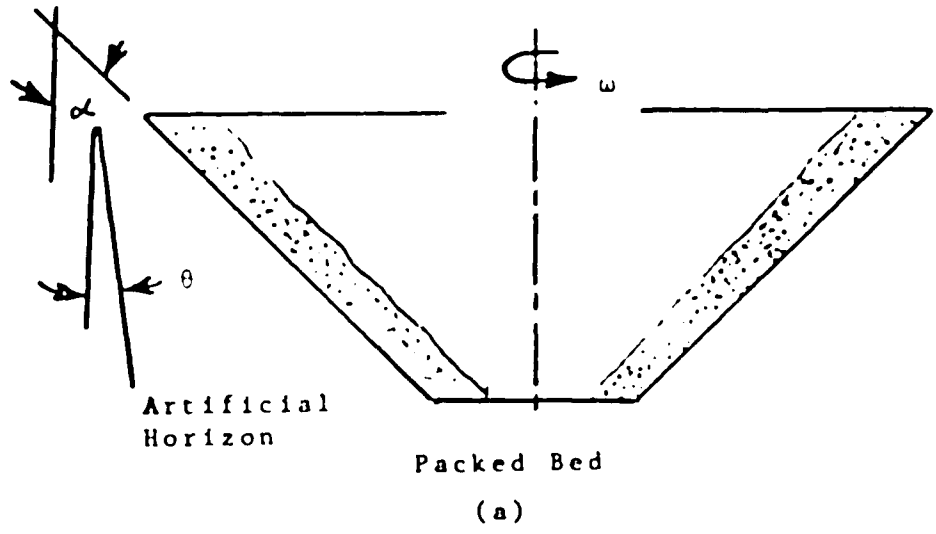

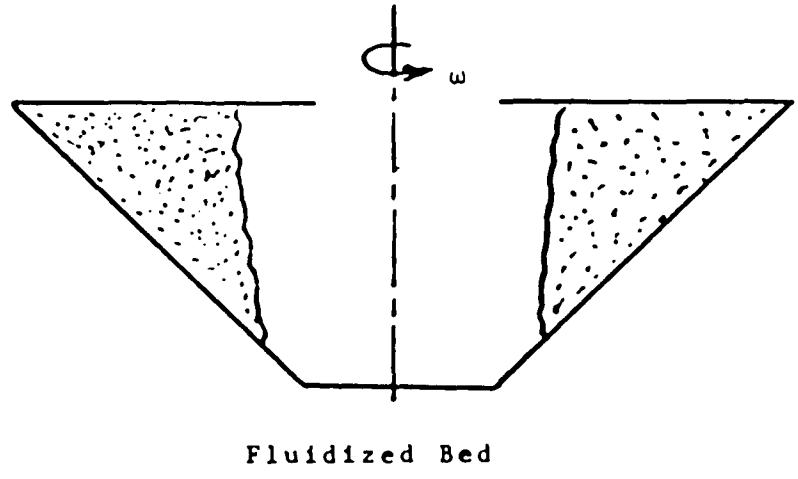

Fig. (D-2) Gross Effect of Grid Taper Angle on Uniformity of Bed Thickness

grid taper angle only infinitesimally larger than the angle between vertical and the artificial horizon (resulted from the centrifugal motion) would allow the distribution over the grid of the fluidized particles, that is for the startup Figure D-2a.

$$\alpha \geq \theta = \arctan\left(\frac{g}{\omega^2 r}\right)$$

Of course, sufficient grid pressure drop must be incorporated in the tapered grid design to insure that elutriation conditions are not reached during the flow of the bed particles toward the top of the grid.

The experiments have shown that the smaller the grid pressure drop, the longer the resulting transition from a packed to an entirely fluidized condition. In fact, with a very low grid pressure drop, transition from minimum fluidization to complete fluidization may require such a large increase in air flow rate that elutriation is reached before total fluidization occurs.

Figures D-3 and D-4 show the axial variation of radial velocity through the bed at minimum fluidization for different grid pressure drops. These results indicate that a low grid resistance causes extremely large axial variations in velocity. As the grid flow resistance approaches zero, the velocity nonuniformity

is large enough to permit elutriation to occur immediately, after the first peripheral ring of bed material is fluidized. Figure D-5 shows the theoretical effects of a grid taper on bed pressure drop and minimum fluidization.

From these experiments, a reasonable pressure drop for grid has been found to be

$$\Delta P_{GMF}/\Delta P_{BMF} \geq 0.4$$

for small bed masses, and

$$\Delta P_{GMF}/\Delta P_{BMF} \geq 0.2$$

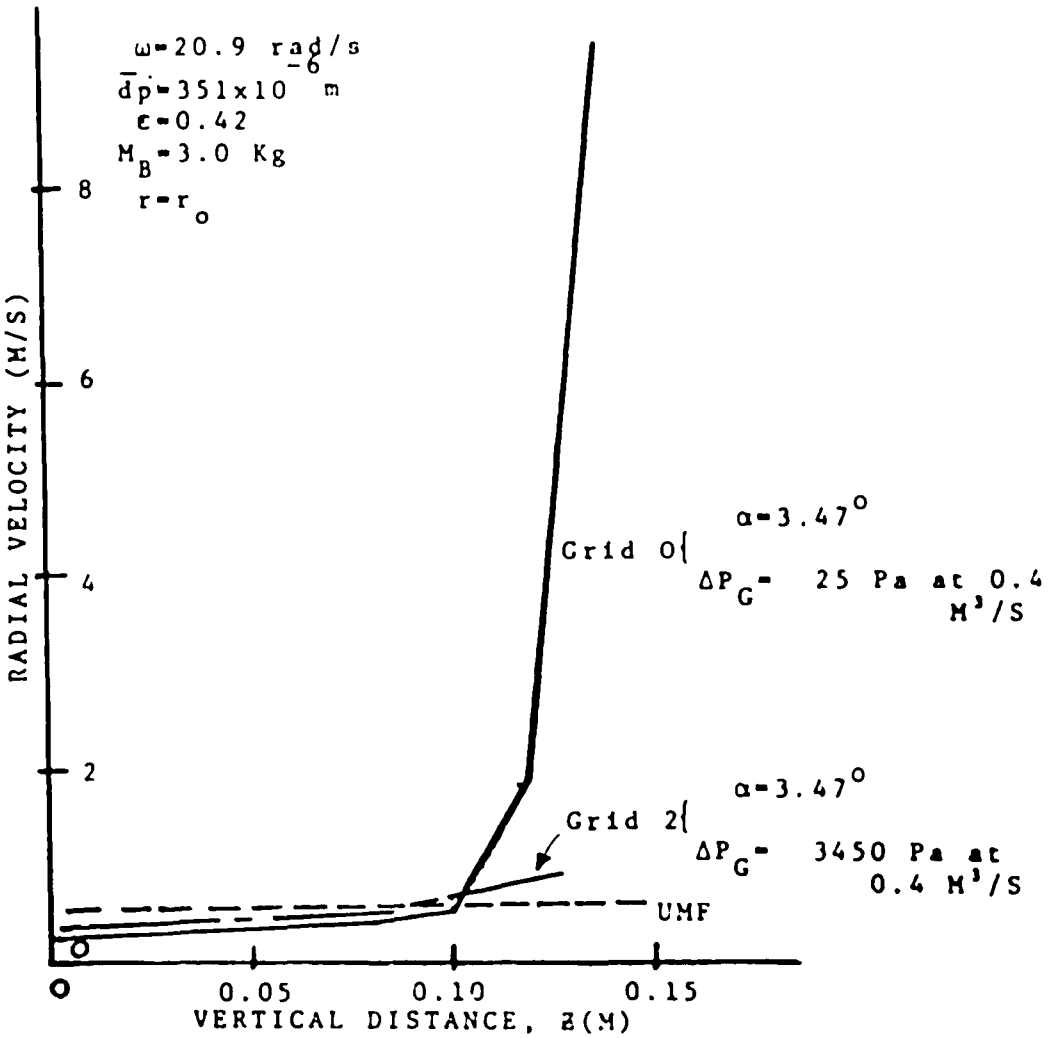

Fig. (D-3) Theoretical Axial Variation of Radial Velocity, Low Angular Velocity

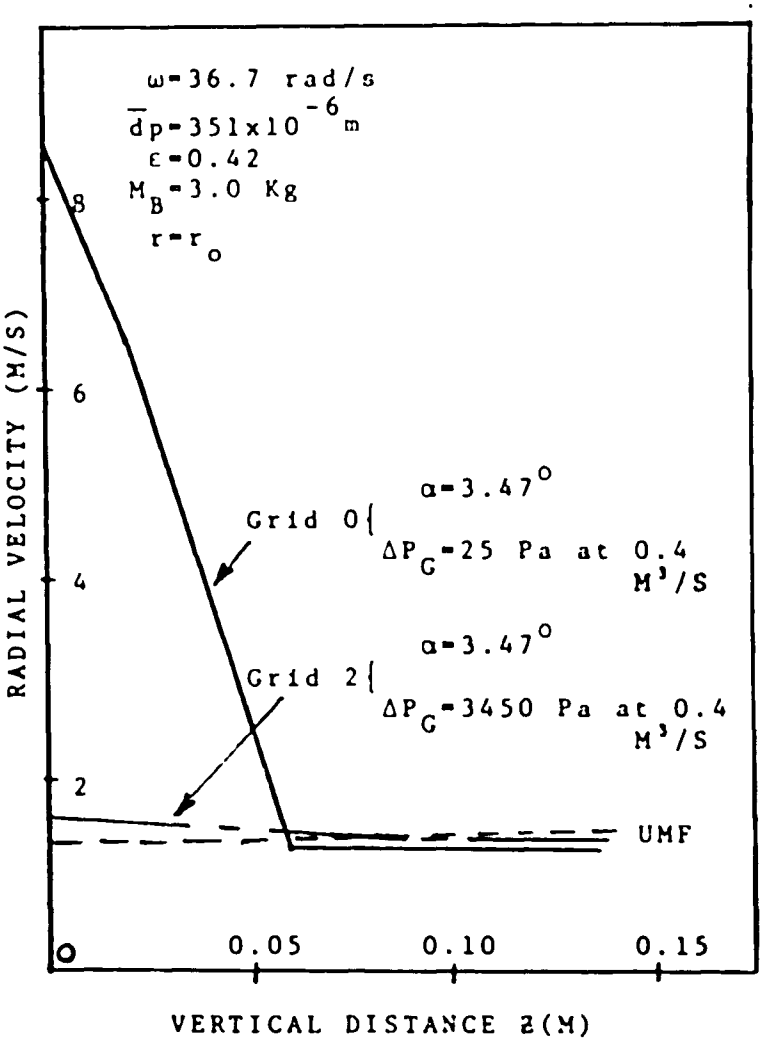

Fig. (D-4) Theoretical Axial Variations of Radial Velocity, High Angular Velocity

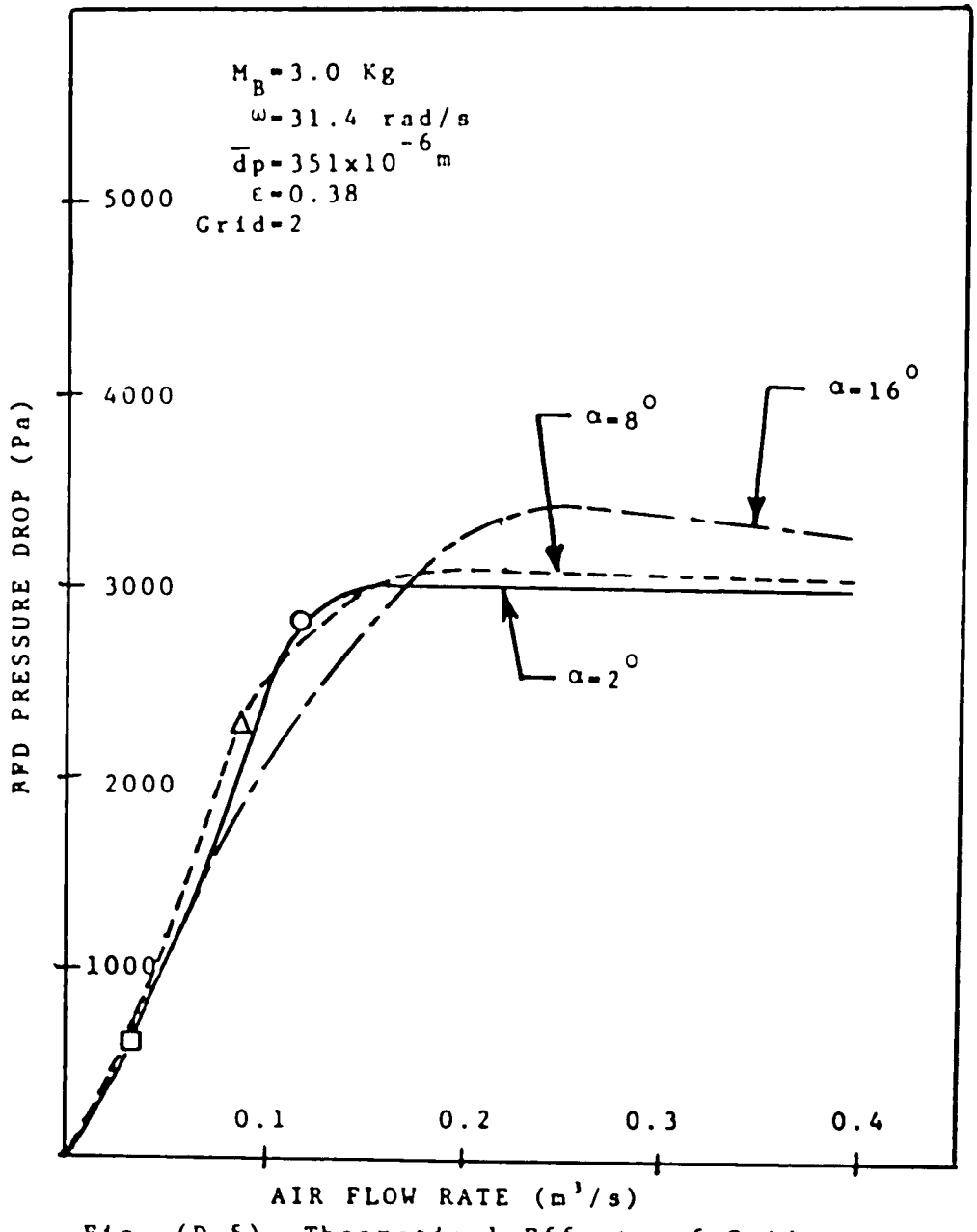

Fig. (D-5) Theoretical Effects of Grid Taper on Bed Pressure Drop and Minimum Fluidization

VITA

Seyed Mohammad Reza Hashemi, the son of Enis and Morteza Hashemi, was born in Teheran, Iran, July 3, 1952. He received a bachelor of science degree in Mechanical Engineering from Teheran University in 1976. He started his graduate studies at Lehigh University in September, 1976 and since then, has been involved in fluidized bed systems and related studies.